# Relativistic Quantum Chemistry for Chemical Identification of the Superheavy Elements

27

Valeria Pershina

## Contents



**Abstract**

Production and investigation of properties of superheavy elements (SHEs) belong to the most fundamental areas of physical science. They seek to probe the uppermost reaches of the periodic table of the elements where the nuclei are extremely unstable and relativistic effects on the electron shells are increasingly strong. Theoretical chemical research in this area is very important. Due to experimental restrictions, it is often the only source of useful chemical information. It enables one to predict the behavior of the heaviest elements in the sophisticated and demanding experiments with single atoms and to interpret their results. Spectacular developments in the relativistic quantum theory and computational algorithms in the last few decades allowed for accurate calculations of electronic structures and properties of SHE and their compounds. Results of those investigations, particularly those related to the experimental research, are overviewed in this chapter. The role of relativistic effects is elucidated.

V. Pershina (✉)
GSI Helmholtzzentrum für Schwerionenforschung GmbH, Darmstadt, Germany
e-mail: V.Pershina@gsi.de

© Springer-Verlag Berlin Heidelberg 2017

W. Liu (ed.), *Handbook of Relativistic Quantum Chemistry*,
DOI 10.1007/978-3-642-40766-6_35

**Keywords**
Predictions of experimental behavior • Quantum chemical calculations • Relativistic effects • Superheavy elements

## Introduction

Superheavy elements (SHEs) are elements with $Z \geq 104$, also called transactinides. They are located in the periodic table after the actinide series ending with element 103, Lr. Nowadays, SHEs from $Z = 104$ through 118 are all known, and most of them have been named (Fig. 1) [1–5].

The SHEs are all man-made. The first members of the transactinides series, $Z = 104$, 105, and 106, were discovered in 1969 through 1974 in heavy-ion accelerators by bombardment of the heavy actinide (Cf) targets with light ions (C and O), so-called "hot-fusion" reactions. In the 1970s, a different type of fusion reactions was found and later used in the production of elements with Z from 106 through 113. These so-called "cold-fusion" reactions were based on targets in the vicinity of doubly magic $^{208}$Pb (mainly Pb and Bi) and beams of the complementary medium-mass projectiles with $Z \geq 24$. The lifetime of the produced elements proved to be very short, for example, the half-life of $^{277}$Cn is only 0.6 ms. The cross section was also found to decrease rapidly with increasing Z. It is, for example, only ~0.5 pb for $^{277}$Cn [2]. It was, therefore, concluded that it would be very difficult to reach even heavier elements in this way. Thus, SHEs from $Z = 112$ through 118 were produced using "hot-fusion" reactions between $^{48}$Ca ions and

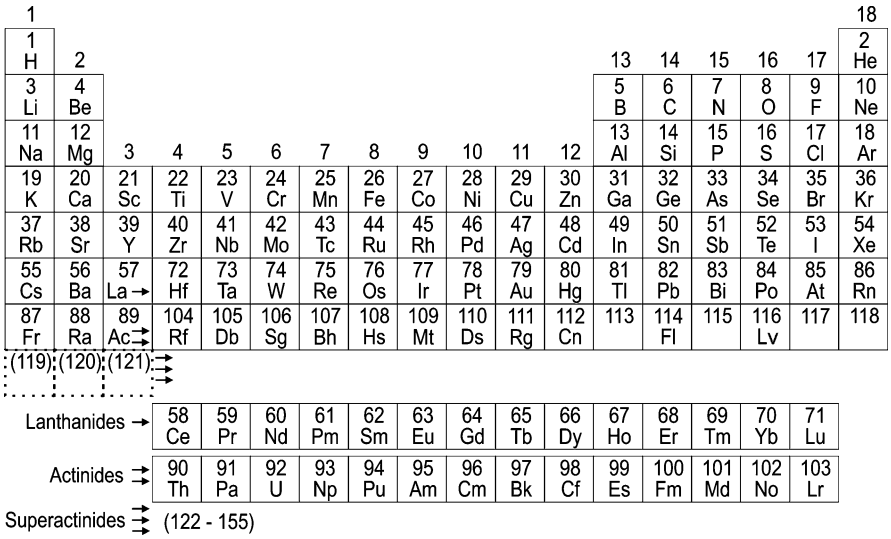


**Fig. 1** Modern periodic table of the elements (Reproduced with permission from Ref. [5]. Copyright 2013 American Chemical Society)

$^{238}$U, $^{242,244}$Pu, $^{243}$Am, $^{245,248}$Cm, $^{249}$Bk, and $^{249}$Cf targets [3]. These discoveries are of considerable interest for chemical studies, because the reported half-lives are much longer (many orders of magnitude) than those of the isotopes produced by "cold-fusion" reactions which lead to more neutron-deficient isotopes, e.g., $t_{1/2}(^{283}\mathrm{Cn}) = 3.8\,\mathrm{s}$ and $t_{1/2}(^{289}\mathrm{Fl}) = 2.1\,\mathrm{s}$.

For the positive identification of a new element and its placement in a proper position in the periodic table, its atomic number, $Z$, must be determined or deduced in some way. For the transactinides up to $Z = 113$, their atomic number has been identified first by "physical" techniques. One widely used technique is that of $\alpha\alpha$ – correlation of the element's $\alpha$-decay to a known daughter and/or granddaughter nucleus. Positive identification becomes more difficult for species that decay predominantly by spontaneous fission. Also, neutron-rich isotopes of elements beyond $Z = 113$ decay into unknown products, so that their $Z$ cannot be directly established. One of the indirect ways of determining $Z$ in that area is by measuring X-ray spectra along the scheme established for element 115 [4].

But even when the atomic number can be positively assigned by $\alpha$-decay chains, no knowledge is obtained about electronic configurations or chemical properties of these new elements from these physical methods. The elements are just placed in the periodic table in corresponding chemical groups or periods according to their $Z$. Thus, it is a matter of chemistry, both theoretical and experimental, to validate or contradict such a placement [5]. It is also essential to establish whether trends in properties observed in the chemical groups for the lighter elements is continued with SHE or whether deviations occur due to the increasingly important relativistic effects.

Due to the instability of isotopes of these elements and low production rates, experimental chemical research in this area is very demanding. Chemical experiments are usually designed so that the behavior of the unknown isotope is compared to that of lighter homologs in the chemical group in order to assess their similarity. Such experiments are restricted to measurements of only few properties – volatility and complex formation. Electronic ground-state configurations, lying in the basis of the periodicity, ionization potentials (IPs), electron affinities (EAs), and many other properties, cannot be measured for SHE. Even a chemical composition of SHE species is assumed in experimental studies by analogy in the behavior with that of their lighter homologs in the groups. Thus, in the area of the heaviest elements, chemical theory becomes extremely important and is often the only source of useful information. It also aims at predicting an outcome of sophisticated experiments with single atoms and interpreting their results. Finally, it is only the theory that can reveal relativistic effects influence on chemical properties of SHE: only by comparing the observed behavior with that predicted on the basis of relativistic *vs* nonrelativistic calculations can the importance and magnitude of relativistic effects be established.

In the past, predictions of chemical properties of the heaviest elements were made with the help of relativistic atomic calculations and extrapolations of the periodic trends [6,7]. Due to recent developments in the relativistic quantum theory, calculation algorithms, and computer techniques, very accurate calculations for

SHE and their compounds became possible. On their basis, reliable predictions of SHE properties and experimental behavior required for their chemical identification have been made. Examples of these studies are given in this chapter. Some latest reviews on this subject are those of [5, 8–11].

## Relativistic and QED Effects on SHE

The relativistic mass increase for a particle (an electron) with velocity $v$ is

$$m = m_0 \left[(1 - (v/c)^2\right]^{-1/2} \tag{1}$$

where $m_0$ is the mass at zero velocity (rest mass) and $c$ is the speed of light. The Bohr model for a hydrogen-like species gives the following expressions for the velocity, energy, and orbital radius of an electron:

$$v = (2\pi e^2/nh)Z; \tag{2}$$

$$E = -(2\pi^2 e^4/n^2h^2)mZ^2; \tag{3}$$

$$r = Ze^2/mv^2, \tag{4}$$

where $n$ is the principal quantum number, $e$ is the charge of the electron, and $h$ is Planck's constant. For SHE, $m/m_0$ is dramatically enlarging. It is, e.g., 1.79 for Fl and 1.95 for element 118. As a consequence, all the three relativistic effects on the valence AOs – contraction and stabilization of the s and $p_{1/2}$ AOs, expansion and destabilization of the $p_{3/2}$, d, f, and g AOs, and the spin-orbit (SO) splitting of AOs with $l > 0$ – are also very large for SHE. Figure 2 shows, e.g., the relativistic stabilization of the ns and $np_{1/2}$ AO and the SO splitting of the np AOs of group-14 elements, with the latter reaching 50 eV for element 164 [6].

For element 112, Cn, the 7s AO is 10 eV relativistically stabilized and 25 % contracted (Fig. 3). At this element, the relativistic contraction and stabilization of the 7s AOs reach their maximum in the seventh row of the periodic table [10].

In the 6d series, the relativistic destabilization and the SO splitting of the 6d AOs increase. Together with the stabilization of the 7s AO, this results in an inversion of the 7s and $6d_{5/2}$ energy levels at Cn, so that its first ionized electron is $(n-1)d_{5/2}$, but not the ns one as in Hg (Fig. 3). (The inversion of the 7s and $6d_{5/2}$ levels in the 7th row starts already at element 108, Hs.) The example of group-12 elements also shows that trends in the relativistic and nonrelativistic energies and $R_{max}$(ns) AOs (the same is valid for the $np_{1/2}$ AOs) are opposite with increasing $Z$ in the groups, which results in opposite trends in relativistic and nonrelativistic properties of the elements defined by those AOs.

In the 7p series, the $7s^2$ pair is so stabilized that it becomes practically an inert core (Fig. 2). The 7p AO SO splitting is also very large: 4.7 eV for Fl and 11.8 eV for element 118 [12]. The relativistic stabilization and contraction of the 8s AO of

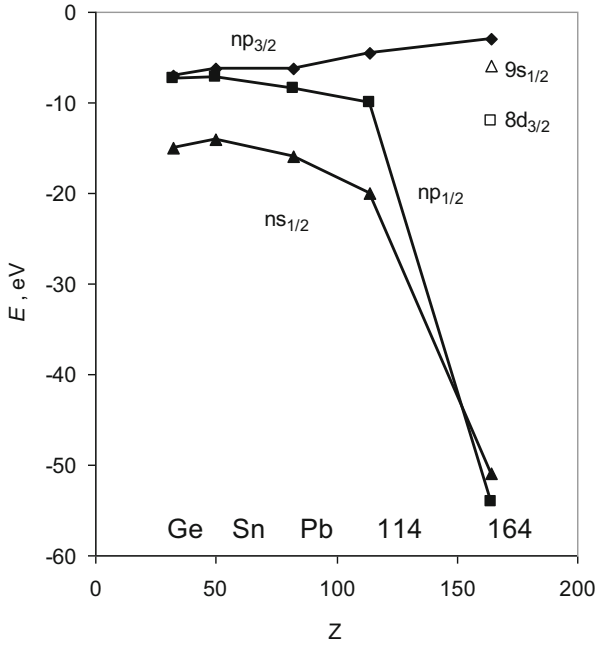


**Fig. 2** Dirac-Slater eigenvalues of the valence electrons of group-14 elements in the $sp^2p$ configuration (Redrawn from [6])

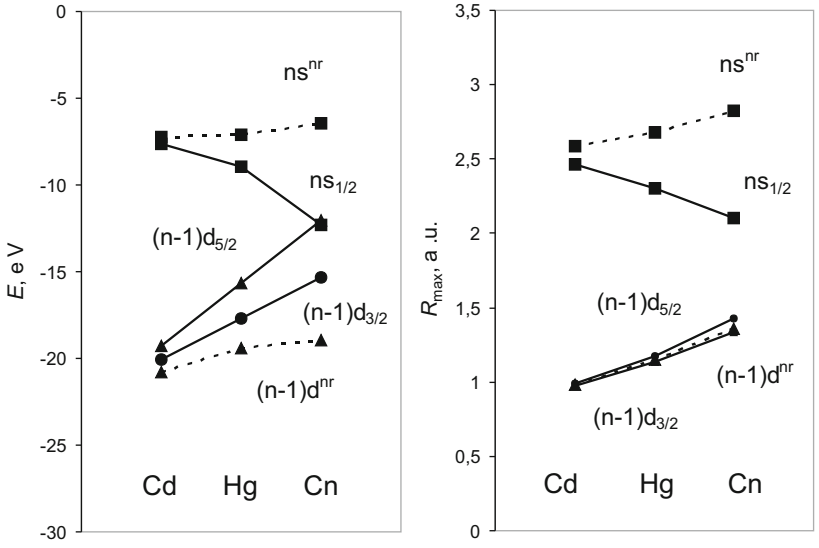


**Fig. 3** Relativistic (*solid line*) and nonrelativistic (*dashed line*) energies and the maximum of the radial charge density, $R_{max}$, of the valence 7s and 6d AOs. The Dirac-Fock data are from [12] (Reprinted with permission from Ref. [11]. Copyright 2011 Oldenbourg Wissenschaftsverlag GmbH)

elements 119 and 120 are also enormous, so that they should behave like K and Ca, respectively. For the heavier elements, relativistic effects are even more pronounced and could lead to properties very much different from those of the lighter homologs [6]. Without relativistic effects the properties would, however, have been also very much different due to the diffuse valence s- and p-AOs and compact d, f, and g AOs [10].

Breit effects accounting for magnetic and retardation interactions on valence orbital energies and IP of the heaviest elements are small, for example, only 0.02 eV for element 121. They can, however, reach a few % for the fine-structure-level splitting in the 7p elements and are of the order of correlation effects there. In element 121, they can be as large as 0.1 eV for transition energies between states including f AOs [13].

Quantum electrodynamic (QED) effects, such as vacuum polarization and electron self-energy, are known to be very important for inner shells, for example, in accurate calculations of X-ray spectra. For the valence shells, the Breit and Lamb-shift terms were shown to behave similarly to the kinetic relativistic effects scaling as $Z^2$ [14]. For the group-11 and group-12 valence s-shells, the increase with $Z$ is even larger. The nuclear volume effect grows faster with $Z$. Consequently, for SHE, its contribution to the orbital energy will be the second important one after the relativistic contribution. Thus, e.g., for element 118, QED effects on the binding energy of the 8s electron cause a 9 % reduction (0.006 eV) of EA [15]. QED corrections for some SHE are given in [16].

## Chemical Experiments

Due to the short half-lives of SHE isotopes and low production rates, special techniques had to be developed that allow for measurements of macrochemical properties of these elements on the basis of single-atom events. Chemical separations in which a single atom rapidly participates in many identical chemical interactions to two-phase systems with fast kinetics that reach equilibrium quickly turned out to be appropriate. Thus, it is sufficient to combine results of many separate "one-atom-at-a-time" experiments or identical experiments with only one atom, in order to get statistically significant results. Two main types of experimental techniques – gas phase and liquid chemistry chromatography – are based on this principle.

- Gas-Phase Chemistry

Gas-phase chemistry deals with the study of volatility of the heaviest elements or their compounds [5, 8, 17, 18]. In macrochemistry, a measure of volatility of a substance is its sublimation enthalpy, $\Delta H_{sub}$. In the gas-phase chromatography, a measure of volatility is the adsorption enthalpy, $\Delta H_{ads}$, of a species on the surface of gold- or $SiO_2$-plated detectors located along the chromatography column. (Gold is chosen as it is free from oxide layers.) The obtained $\Delta H_{ads}$ are then used to

deduce $\Delta H_{\text{sub}}$ via a loose correlation between these quantities. Many assumptions are involved in this approach.

There are two kinds of such techniques. In the first one, *thermochromatography*, a longitudinal, negative temperature gradient (from about room temperature down to about −180 °C), is established along the chromatography column through which a gas stream is conducted. It contains volatile species of interest (atoms or molecules) that deposit on the surface of the column according to their volatilities. The deposition zones are registered by detectors, which are associated with specific deposition (adsorption) temperatures, $T_{\text{ads}}$ (Fig. 4, left panel). The obtained $T_{\text{ads}}$ are then used to deduce the adsorption enthalpy, $\Delta H_{\text{ads}}$, using adsorption models and Monte Carlo simulations [17].

In another technique, *isothermal chromatography*, the entire column is kept at a constant temperature. Volatile species pass through the column undergoing numerous adsorption-desorption steps on the surface of the column, usually made of quartz. Their retention time in the column is indicative of their volatility at a given temperature. A series of temperatures is run, and the chemical yield of the species is studied as a function of the temperature (Fig. 4, right panel). A temperature, $T_{50\,\%}$, at which 50 % of the species pass through the column is taken as a measure of volatility in a comparative study. A Monte Carlo program is used to deduce $\Delta H_{\text{ads}}$ from the measured $T_{50\,\%}$ using adsorption models [17].

Both techniques were used to study volatility of compounds of Rf through Hs and of atoms of Cn and Fl, whose isotopes have half-life, $t_{1/2}$, of the order of at least one second [2, 5, 18].

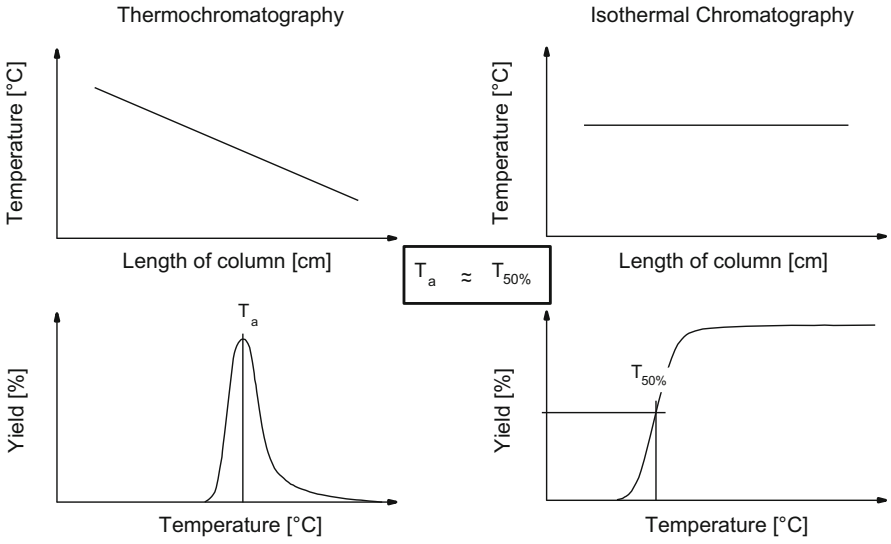


**Fig. 4** *Upper panel*, temperature profiles employed in thermochromatography and isothermal chromatography, and *lower panel*, deposition peak and integral chromatogram resulting from thermochromatography and isothermal chromatography, respectively (Reprinted with permission from Ref. [18]. Copyright 2003 Kluwer Academic Publishers)

- Aqueous chemistry

To study complex formation of the heaviest elements and their homologs in aqueous solutions liquid-liquid or ion (cation, CIX, or anion, AIX) exchange chromatography fast separation techniques have been developed [19]. They allow for measurements of the distribution coefficient, $K_d$, between aqueous and organic phases:

$$K_d = \frac{K_{DM}[RB^+L^-]^p_{\text{org}}\beta_i\,[L^-]^{i-p}}{\sum\limits_0^N \beta_n\,[L^-]^n}, \tag{5}$$

where $\beta_i$ is the complex formation constant. Obtained $K_d$ (usually plots of $K_d$ values *vs* acid concentration) are used to judge about stabilities of the formed complexes, $\beta_i$. In experiments with radioactive species, $K_d$ is measured as a ratio of the activity of the studied species in the organic phase to that in the aqueous phase. It is closely related to the key observable, the retention time, $t_r$, in the chromatography column:

$$K_d = (t_r - t_0)\frac{V}{M}, \tag{6}$$

where $t_0$ is the column holdup time due to the free column volume, $V$ is the flow rate of the mobile phase, and $M$ is the mass of the ion exchanger.

Aqueous chemistry experiments that are more time-consuming than the gas-phase ones, mainly because of the time needed for the preparation of a sample suitable for $\alpha$-spectroscopy, require isotopes with longer $t_{1/2}$, of the order of minutes. Therefore, only complex formation of Rf, Db, and Sg has been studied so far [19].

## Relativistic Quantum Chemical Methods and Approaches

- Relativistic quantum chemical methods

For reliable predictions of SHE properties, quantum chemical methods should treat relativistic and correlation effects at the highest possible level of theory. A short description of the relativistic methods is given below. Comprehensive reviews can be found in [20, 21], as well as in this issue.

**Wave-function-based (ab initio) methods**. The most straightforward way to solve the Dirac many-electron equation

$$h_{\text{DCB}} = \sum_i h_D(i) + \sum_{i<j}\left(1/r_{ij} + B_{ij}\right), \tag{7}$$

where the one-electron Dirac operator is

$$h_D(i) = c\vec{\alpha}_i \vec{p}_i + c^2(\beta_i - 1) + V^n(i), \tag{8}$$

and $\vec{\alpha}$ and $\beta$ are the four-dimensional Dirac matrices, $V^n$ is the nuclear attraction operator, and the Breit term in the low photon frequency limit is

$$B_{ij} = -1/2\lfloor(\vec{\alpha}_i \vec{\alpha}_j) r_{ij}^{-1} + (\vec{\alpha}_i \vec{r}_{ij})(\vec{\alpha}_j \vec{r}_{ij}) r_{ij}^{-3}\rfloor, \tag{9}$$

is that without approximations. The operators of the Dirac equation (7) are $4 \times 4$ matrix operators, and the corresponding wave function is therefore a four-component (4c) vector (spinor). The $V^n$ includes the effect of the finite nuclear size, while some finer effect, like QED, can be added to $h_{\mathrm{DCB}}$ perturbatively, although the self-energy QED term is more difficult to treat. The DCB Hamiltonian in this form contains all the effects through the second order in $\alpha$, the fine-structure constant.

Since the relativistic many-body Hamiltonian cannot be expressed in closed potential form, which means it is unbound, projection one- and two-electron operators are used to solve this problem. The operator projects onto the space spanned by the positive-energy spectrum of the Dirac-Fock-Coulomb (DFC) operator. In this form, the "no-pair" Hamiltonian is restricted then to contributions from the positive-energy spectrum and puts Coulomb and Breit interactions on the same footing in the SCF calculation [22]. The proper way to go beyond the "no-pair" approximation has recently been discussed by Liu [23].

Because the Dirac equation is written for one electron, the real problem of ab initio methods for a many-electron system is an accurate treatment of electron correlation. The latter is of the order of magnitude of relativistic effects for binding energies and other properties. The DCB Hamiltonian (Eq. 7) accounts for these effects in the first order via the $V_{ij} = 1/r_{ij}$ term. Some higher orders of magnitude correlation effects are taken into account by the configuration interaction (CI) and many-body perturbation theory (MBPT) techniques, including the Møller-Plesset (MP) theory, or, presently, at the highest level of theory, coupled cluster with single-double and perturbative triple, CCSD(T), excitations, or Fock-space CC (FSCC) techniques [13, 24, 25].

The problems of electron correlation and proper basis sets make the usage of the 4c ab initio DF(C) methods rather limited in molecular calculations. These methods are still too computer time intensive and are not sufficiently economic to be applied to the heaviest elements in a routine manner, especially to the complex systems studied experimentally. Mostly small molecules, like hydrides or fluorides of SHE, were calculated with their use. The DC method is also implemented in the DIRAC program package [26].

**Two-component (2c) methods**. Due to the practical limitations of the 4c methods, the 2c ones are very popular in molecular calculations. In this approximation, the "positronic" and electronic solutions of the Dirac-Hartree-Fock (DHF) method are decoupled. This reduces the number of matrix elements in the Hamiltonian to inter-

actions solely among electrons (positive-energy states) and nuclei and, therefore, saves valuable computer time. Perhaps, the most applied method of decoupling the large and small components of the wave function is the Douglas-Kroll-Hess (DKH) approximation [27]. The 2c Hamiltonians often used in molecular applications are X2C [28–31] and BSS [32], also implemented in the DIRAC program package [26]. A comprehensive review on the X2C methods is that of [29].

*Effective core potentials* (ECPs) allow for more economic calculations within the DHF schemes by replacing inner core orbitals that do not take part in the bond formation by a special (effective core) potential. In this way, the number of basis functions and, therefore, two-electron integrals is drastically diminished. There are ECPs of two main types, as well as pseudo-potentials (PPs) and model potentials (MPs). Energy-adjusted PPs known as the Stuttgart ones [33, 34] and the shape-consistent relativistic ECPs (RECPs) [35, 36] are available for SHE. Generalized RECPs accounting for Breit effects have also been developed for some heaviest elements [37].

*Density functional theory* (DFT) is based on the knowledge of the ground-state electron density. Due to the high accuracy and efficiency, computational schemes based on the DFT methods are among the most popular in theoretical chemistry, especially for extended systems, such as large molecules, liquids, or solids [38]. Usually, self-consistent all-electron calculations are performed within the relativistic local density approximation (LDA). The general gradient approximation (GGA), also in the relativistic form (RGGA), is then included perturbatively in $E^{ex}$, the exchange correlation energy functional. The accuracy depends on the adequate knowledge of $E^{ex}$, whose exact form is, however, unknown. There is quite a number of such potentials and their choice is dependent on the system. Thus, PBE is usually favored by the physics community, PBE0, B3LYP, B88/P86, revPBE, etc., and by the chemistry community, while LDA is still used extensively for the solid state.

Spin-unrestricted, or spin-polarized (SP), 4c-DFT methods allowing for accurate calculations of open-shell systems are those of Anton et al. [39], the Beijing group (BDF) [40], and ReSpect [41]. The first two were extensively used for SHE. They differ by basis set techniques, though they give similar results. The 4c-DFT of Anton et al. [39] allows for treating explicitly very large systems such as clusters of up to more than 100 atoms and is, therefore, suitable for the treatment of adsorption phenomenon on surfaces of solids.

The 2c-DFT methods are a cheaper alternative to the 4c ones [29, 30, 42, 43]. Quasi-relativistic methods such as the spin-orbit zeroth-order regular approximation (SO ZORA) implemented in the Amsterdam DFT code (ADF) [44] and the DKH method [45] implemented in most program packages are also popular among theoretical chemists. Dispersion-corrected $E^{ex}$ are available in ADF for $Z \leq 92$.

Periodic DFT codes are generally not developed for the SHE: they have neither basis sets nor suitable PP. Also, as a rule (with the exception of RFPLO [46] and ADF-BAND [44]), they are scalar relativistic (SR). In some cases, like, e.g., for calculations of solid Cn and Fl, PPs have been specially developed using the Stuttgart PP model [33]. The ADF-BAND [44] having basis sets for elements up to $Z = 120$ is presently an efficient tool to perform solid-state and adsorption calculations for SHE.

- Approaches used to predict experimentally measurable properties

For weak interactions, e.g., for predictions of the transport of SHE nuclides through Teflon or polyethylene capillaries from the accelerator to the chemistry set up or for the adsorption of volatile species on inert surfaces of a chromatography column, the usage of adsorption models proved to have advantages over direct DFT calculations of adatom-surface interactions. For example, for an atom or a symmetric molecule with a zero dipole moment adsorbed on a dielectric surface, the dispersion interaction energy can be calculated using the following equation coming from an adatom-slab adsorption model [47]:

$$E(x) = -\frac{3}{16}\left(\frac{\varepsilon - 1}{\varepsilon + 2}\right)\frac{\alpha_{\mathrm{mol}}}{\left(\frac{1}{IP_{\mathrm{slab}}} + \frac{1}{IP_{\mathrm{mol}}}\right)x^3}, \tag{10}$$

where $\varepsilon$ is the dielectric constant of the adsorbent material and $x$ is the adatom/molecule – surface distance (usually van der Waals radius). All the atomic or molecular properties of Eq. (10) can be accurately calculated using relativistic codes. Since the detailed structure of the surface of the column is, as a rule, unknown, in a comparative study, it is reasonable to predict $\Delta H_{\mathrm{ads}}$ of a SHE species with respect to the measured $\Delta H_{\mathrm{ads}}$ of a homolog. Thus, $x$ can be deduced from the measured $-\Delta H_{\mathrm{ads}} \approx E_b$ (binding energy) of a lighter homolog using Eq. 10, while $x$ of a species of interest can be estimated using a difference in their van der Waals radii.

In the case of adsorption of atoms on chemically reactive surfaces such as gold or quartz, calculations of $E_b$ can be directly performed either via a cluster model (Fig. 5) using molecular codes or adatom-slab/supercell models using relativistic periodic codes (e.g., ADF-BAND [44]).

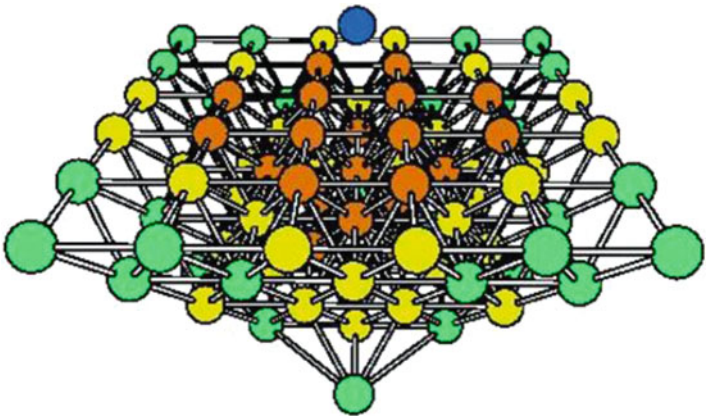

**Fig. 5** A cluster model for the prediction of adsorption (Reprinted with permission from Ref. [9]. Copyright 2014 Springer Verlag)

Various correlations, e.g., between $E_b$ in smaller systems and $\Delta H_{ads}$ or $\Delta H_{sub}$ of substances, turned also out to be useful in predictions of adsorption and sublimation properties of SHE (see below). Knowing then $\Delta H_{ads}$, a relative yield of a volatile species at the end of a capillary or a chromatography column or its $T_{ads}$ can be predicted using a model of mobile adsorption (see [5,9] for reviews).

## Atomic Properties of SHE and the Structure of the Periodic Table

**Electronic configurations**. Ground-state configurations of SHE from Z = 104 through Z = 172 were predicted in the past with the use of DS and DF methods [6,7]. Later, MCDF calculations for neutral and ionized states of Rf through Hs [48, 49] and for grounds states of elements 119 through 164 [50–52] were performed. With the development of CC methods, results of the DC(B) FSCC calculations for Rf and Rg through Fl and for elements 118 through 122 became available (see [13] for a review).

All these calculations have shown that the relativistic stabilization of the 7s AO results in the availability of the $7s^2$ electron pair in the ground states of the 7th row elements, $7s^26d^q$ and $7s^27p^p$. This is in contrast to the 6th row, where Pt and Au have different ground states, $5d^96s$ and $5d^{10}6s$, respectively. For Rf, the MCDF calculations have given the $7s^27p6d$ configuration as the ground state [48]. More accurate DCB FSCC calculations have, however, corrected the MCDF result leading to the $7s^26d^2$ configuration as the ground [13]. A very high level of correlation with $l = 6$ was required to reach this accuracy. For elements 119 and 120, the 8s and $8s^2$ states, respectively, beyond the 118 core were found as most stable. Element 121 has an $8s^28p_{1/2}$ state in the difference to $Ac(7s^26d)$ due to the relativistic stabilization of the $8p_{1/2}$ AO. All these calculations generally agree on the ground states of the elements up to $Z = 122$. They, however, disagree at Z > 122 (Table 1).

Elements beyond the 7th row of the periodic table are characterized by mixing of states coming from partially filled $8p_{1/2,3/2}$, $7d_{3/2,5/2}$, $6f_{5/2,7/2}$, and $5g_{7/2,9/2}$, shells. The proximity of the valence SO bands makes the search for the correct ground state very difficult. The usual classification on the basis of a simple electronic configuration and the placement of these elements in a proper column in this part of the periodic table becomes, therefore, problematic. Thus, the filling of the electron shells and the structure of the periodic table beyond $Z = 122$ are still under discussion and debate (see, e.g., different versions of the periodic table in [6] and [53]). Accurate calculations, preferably using DBC CC + QED techniques,

**Table 1** Ground states of element 121–124 (Z = 120 core +) and 143 (Z = 120 core + $8p_{1/2}^2$+)

| Method | 121 | 122 | 123 | 124 ... | 143 | Ref. |
|---|---|---|---|---|---|---|
| DF | 8p | 7d8p | 6f7d8p | $6f^38p$ | $5g^{17}6f^27d^2$ | [6] |
| DF | 8p | 7d8p | 6f7d8p | $6f^27d8p$ | $5g^{18}7d^3$ | [50] |
| MCDF | 8p | 7d8p | $6f^28p$ | $6f^28p^2$ | $5f^{17}6f^27d^2$ | [51] |
| DCB FSCC | 8p | 7d8p | – | – | – | [13] |

**Table 2** Polarizabilities, $\alpha$ (in a.u.), and ionization potentials, IPs (in eV), of Hg and Cn

| Method | Hg | | Cn | | Ref. |
|---|---|---|---|---|---|
| | $\alpha$ | IP | $\alpha$ | IP | |
| 4c-BDF PBESIC | 36.4 | 10.40 | 29.8 | 11.40 | [54] |
| QR PP CCSD(T) | 34.2 | 10.37 | 28.0 | 13.17 | [54] |
| AR PP CCSD(T) | 34.42 | – | 25.82 | – | [55] |
| ECP CCSD(T) | 28.48 | 10.39 | 28.68 | 11.675 | [56] |
| DC CCSD(T) | 34.15 | 10.445 | 27.64 | 11.97 | [57,58] |
| Exp. | 33.919 | 10.4375 | | | [59] |

are, therefore, highly needed in this area to resolve the contradictions. At the time being, advanced MCDF calculations including QED effects [52] confirmed earlier predictions from single-configuration DF calculations [6] about the end of the periodic table at $Z = 173$, when the energy of the 1s level becomes less than $-2mc^2$.

**Ionization potentials**. Various calculations – DF, DS, MCDF, and DC(B) CC – of IPs were performed for elements 104 through 166 (see [6–9, 13, 54–58]). The accuracy upon approximation is shown in Table 2 for Hg and Cn, as an example, with the DC CCSD results [57,58] being the most accurate.

The influence of relativistic effects on IP and other atomic properties of group-12 elements is shown in Fig. 6, as an example. The relativistic IPs are larger than the nonrelativistic ones, and they increase in group 12, with the maximum at Cn. Nonrelativistically, IP(Cn) would have been about that of Cd. Relativistic effects act similarly on elements 113 and 114, i.e., they cause an increase in IPs due to the relativistic stabilization and contraction of the $np_{1/2}$ AO. On the contrary, in groups 15 through 18, IPs decrease with atomic number due to the destabilization of the $np_{3/2}$ AO, so that DC FSCCSD IP(118) of 8.914 eV [60] is smaller than IP(Rn) of 10.799 eV [59].

Especially interesting are trends in properties of group-1 and group-2 elements, having the ns and $ns^2$ ground states, respectively. The trends in IP are reversed in groups 1 and 2 at Cs and Ba, respectively (Fig. 7) due to the trend reversal in the energies of the ns AOs. Thus, IP(119) should be about IP(K), and IP(120) should be about IP(Ca).

**Electron affinities**. EAs were calculated for a few of the heaviest elements. No bound anion was found for Cn by the DCB FSCC calculations [58]. Fl was shown to have no EA at the DC FSCC level of theory either [61]. On the contrary, element 118 has a positive EA of 0.058 eV, according to the DCB FSCC + QED calculations [15]. This is a result of the 8s AO relativistic stabilization.

EAs of group-1 and group-2 elements, like their IPs, show a reversal of the trends from the 6th row on, however, group 1 behaves differently from group 2. Thus, in group 1, the trend to a decrease in EA at the lighter elements is changed at Cs to an *increase* toward element 119 (Fig. 7), while in group 2, the trend to an increase at the lighter elements is changed at Ba to a *decrease* toward element 120. These opposite

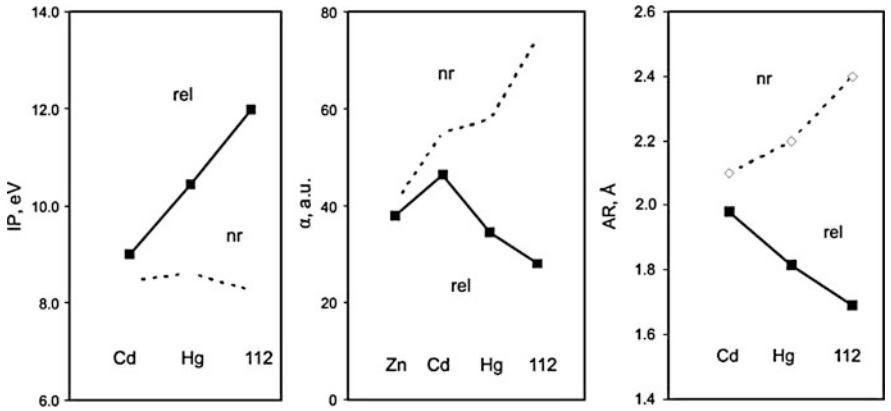


**Fig. 6** Relativistic (*solid lines*) and nonrelativistic (*dashed lines*) ionization potentials (IPs), atomic radii (AR), and polarizabilities, $\alpha$, of group-12 elements (Reprinted with permission from Ref. [47]. Copyright 2005 Elsevier)

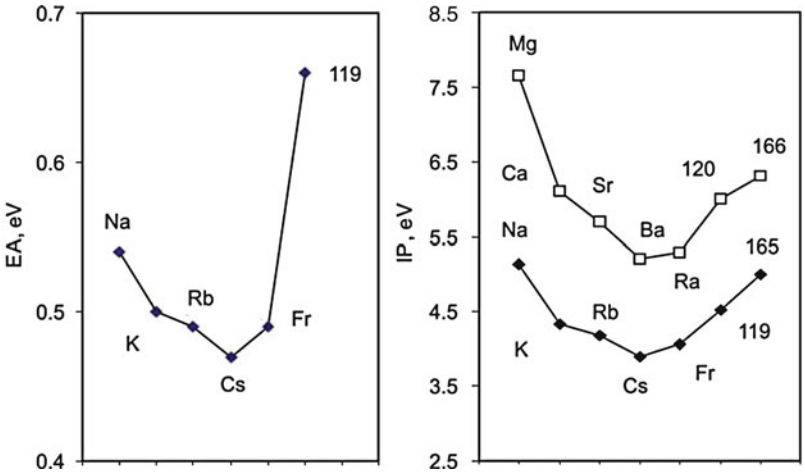


**Fig. 7** Electron affinities, EAs, and ionization potentials, IPs, of alkali and alkaline-earth elements. The data for Na through Fr and Mg through Ra are experimental

trends in EA in groups 1 and 2 are due to the opposite trends in the energies of *different* AOs responsible for the electron acceptance process – the ns AOs in the former case and the $np_{1/2}$ + (n−1)d AOs in the latter. It was also shown that inclusion of the triple excitations (T) in the CC procedure for the electron correlation is crucial in stabilizing the 120 anion: the RCCSD(T) result is 21 meV, while the DHF result (without correlation) is much worse, −121 meV (Table 3) [62]. The EA of element 121 is the highest in group 3 due to the relativistic stabilization of the $8p_{1/2}$ AO [13].

**Table 3** Electron affinity of group-2 elements calculated within different approximations [62]

| Elem. | State | DHF | RCCSD | RCCSD(T) | Exp. |
|---|---|---|---|---|---|
| Ba | $6s^2 6p$ | −0.143 | 0.070 | 0.138 | 0.144 |
| Ra | $7s^2 7p$ | −0.099 | 0.042 | 0.082 | > 50 |
| 120 | $8s^2 8p$ | −0.121 | −0.002 | 0.021 | – |

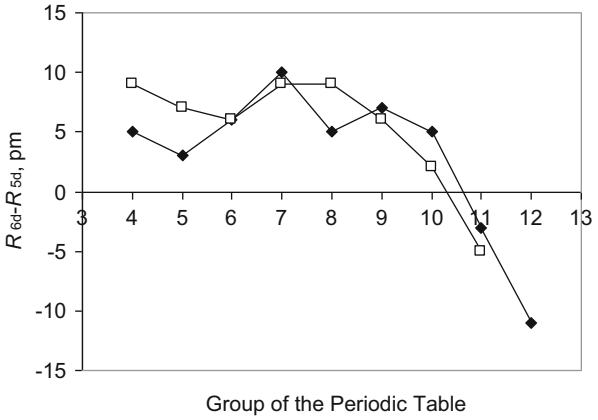


**Fig. 8** The difference in the lengths of the single (*filled rhomboids*) and triple (*open squares*) bonds between the 6d and 5d metals (Reproduced with permission from Ref. [53]. Copyright 2011 Royal Society of Chemistry)

**Atomic/ionic/covalent radii**. Atomic (AR) and ionic (IR) radii of SHE were predicted using DS/DF and MCDF calculations of $R_{\max}$ of the charge density of outer AOs [6,48,49]. A set of atomic single- and triple-bond covalent radii (CR) for most of the elements of the periodic table including the heaviest ones till Z = 118 and 112, respectively, is also suggested in [63]. They were obtained from calculated bond lengths, $R$, in simple compounds. All the results show that the CR of the group 4 – 8 6d elements – are about 0.5–0.8 Å larger than those of the 5d elements. An important finding of these works is a decrease in the $R_{6d} - R_{5d}$ difference starting from group 9, reaching negative values in groups 11 and 12, as a result of the increasing 7s AO contribution (Fig. 8). This is called a "transactinide break" [63]. The relativistic AR contraction of Cn is also shown in Fig. 6.

In groups 13 and 14, AR also decrease with $Z$ due to the relativistic contraction of the $7p_{1/2}$ AOs, while in groups 15 through 18, they increase with $Z$ due to the relativistic expansion of the $np_{3/2}$ AOs.

**Polarizabilities**. Static dipole polarizabilities, $\alpha$, were calculated at various levels of the relativistic quantum theory for Cn through element 119 (see [9] for a review). Table 2 shows results of various calculations for Hg and Cn [54–57]. According to the calculations, $\alpha$(Cn) should be the smallest in group 12 due to the relativistic contraction of the outer 7s AO (Fig. 6). Correlation effects were shown to decrease $\alpha$ in Hg, Cn, and Pb and to increase it in Fl. Thus, one can see that exclusively due to

relativistic effects, Cn should be chemically rather inert, much more than the lighter homologs in group 12, while element 118 should be chemically most reactive in group 18, having a DC CCSD(T) $\alpha$ of 46.33 a.u., larger than $\alpha$(Rn) of 35.04 a.u. [60].

The calculated atomic properties were used to predict the transport of single atoms from the accelerator to the chemistry setup though Teflon capillaries. Using Eq. (10), $-\Delta H_{ads}$ of elements 113, 114, 118, and 120 were obtained as 14, 10.4, 10.8, and 35.4 kJ/mol, respectively, ensuring their safe delivery [11, 57, 60, 62]. The relative yield of SHE at the end of the transport system has also been given using the $\Delta H_{ads}$. Thus, e.g., for the $^{300}120$ isotope with $t_{1/2} = 1$ s and $-\Delta H_{ads}(120) = 35.4$ kJ/mol, the relative yield is calculated as 90 % and 60 % for an open Teflon column or a capillary with an inner diameter of 2 mm and a length of 1 m and 10 m, respectively, and a gas volume $Q = 1$ l/mol at room temperature [62]. Thus, for this element, the limiting factor for the delivery is not its volatility, but the short half-life.

## Gas-Phase Chemistry

**Groups 4–8, common features**. Elements at the beginning of the 6d series were shown to form volatile halides, oxyhalides, and oxides by analogy with their lighter homologs in groups 4–8. With the aim to predict their stability and volatility, calculations for the following species – $MF_4$, $MCl_4$, $MOCl_2$, $MBr_4$ (M = Zr, Hf, and Rf), $MCl_5$, $MBr_5$, $MOCl_3$ (M = Nb, Ta, and Db), $MCl_6$, $MO_3$, $MOCl_4$, $MO_2Cl_2$, $M(CO)_6$ (M = Mo, W, and Sg), $MO_3Cl$ (M = Tc, Re, and Bh), $MO_4$ (M = Ru, Os, and Hs), and MX (M = Rf – Cn, X = H, N, B, and C) – were performed with the use of relativistic DFT and CC methods. (A full list of calculated properties is given in Tables 8 and 9 of [9]). The calculations confirmed that compounds of Rf through Hs are homologs of the lighter congeners in the chemical groups and that bonding is due to the participation of the 6d and 7s AOs. An increase in covalence (a decrease in effective metal charges, $Q_M$, and an increase in overlap population, OP), as well as in the stability of the maximum oxidation state in the groups has been established. It was shown to be a relativistic effect (Fig. 9) [9].

The atomization energies, $D_e$, of the 6d-element molecules turned out to be smaller than $D_e$ of the lighter homologs due to the larger SO effects and a smaller ionic contribution. Thus, e.g., SP 4c-DFT $D_e(RfCl_4)$ is 19.53 eV, smaller than $D_e(ZrCl_4)$ of 21.7 eV and $D_e(HfCl_4)$ of 21.1 eV [9]. Electron correlation is proven to contribute to more than 50 % to bonding in the SHE systems (see Table 5 below). Electron correlation and relativistic effects were shown to be nonadditive.

**Group 4**. In the difference to expectations, an unusual trend in volatility has been observed for group-4 halides, $ZrCl_4 \approx RfCl_4 > HfCl_4$ and $ZrBr_4 \approx RfBr_4 > HfBr_4$, using isothermal gas-phase chromatography with a quartz column (Fig. 10) (see [5] for a review).

To interpret this unusual behavior and to prove stability of the halide and oxyhalide of Rf, 2c- and 4c-DFT calculations were performed for $MCl_4$ and $MOCl_2$

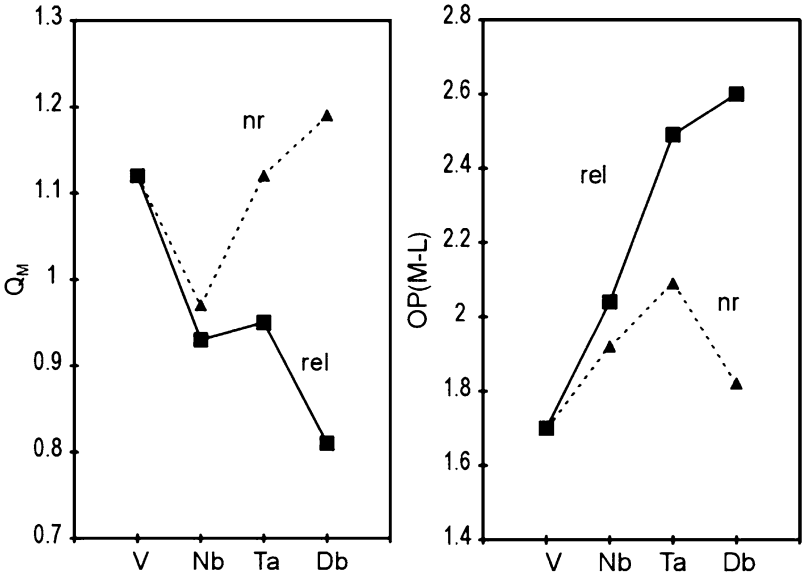


**Fig. 9** Relativistic (*solid lines*) and nonrelativistic (*dashed lines*) effective charges, $Q_M$, and overlap populations, OP, for $MCl_5$ (M = V, Nb, Ta, and Db). L denotes the ligand (Reprinted with permission from Ref. [9]. Copyright 2014 Springer Verlag)

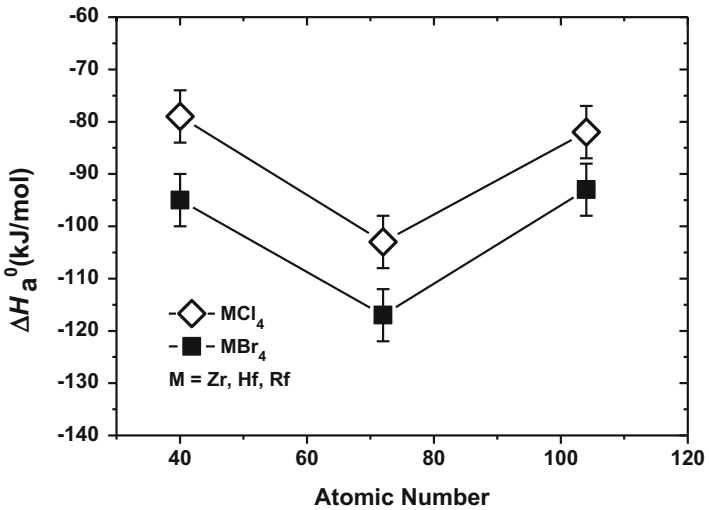


**Fig. 10** Adsorption enthalpies of group-4 tetrachlorides and tetrabromides (Reproduced with permission from Ref. [5]. Copyright 2013 American Chemical Society)

**Table 4** The X2C (B88/P86) calculated properties of $MCl_4$ (M = Zr, Hf, and Rf): equilibrium bond lengths, $R_e$ (in Å); atomization energies, $D_e$ (in eV); ionization potentials, IPs (in eV); polarizabilities, $\alpha$ (in a.u.); as well as adsorption enthalpies, $\Delta H^\circ_{ads}$ (in kJ/mol), on a quartz surface and sublimation enthalpies, $\Delta H^\circ_{sub}$ (in kJ/mol), of bulk

| Molecule | $R_e$ | $D_e$ | IP | $\alpha$ | $\Delta H^{\circ a}_{ads}$ | $\Delta H^{\circ b}_{ads}$ | $\Delta H^{\circ c}_{sub}$ |
|---|---|---|---|---|---|---|---|
| $ZrCl_4$ | 2.336 | 20.34 | 11.00 | 103.6 | 106.5 | 97 | 110.5 |
| $HfCl_4$ | 2.316 | 20.80 | 11.00 | 99.3 | 103 | 103 | 104.7 |
| $RfCl_4$ | 2.370 | 19.40 | 10.96 | 101.2 | 102.7 | 87 | (104.2)[a] |

[a]Theory [64, 65]
[b]Experiment (see [5] for references)
[c][59]

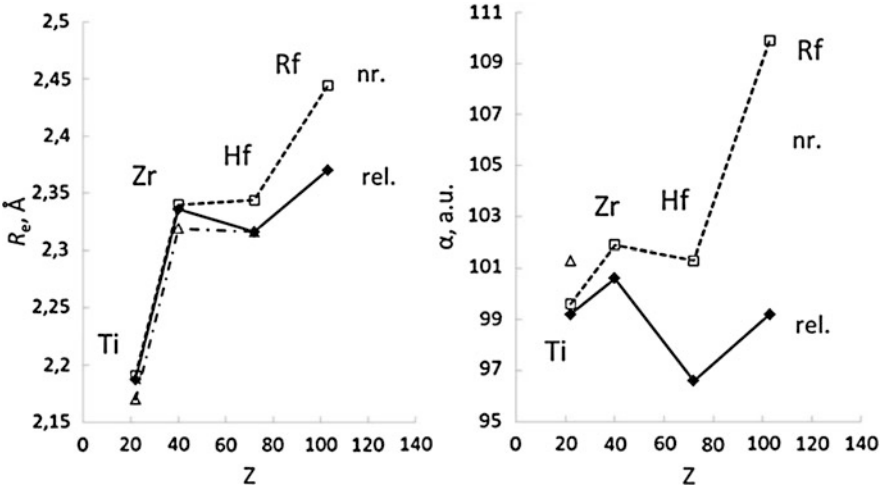


**Fig. 11** Relativistic (*solid lines*) and nonrelativistic (*dashed lines*) bond lengths, $R_e$, and polarizabilities, $\alpha$, of $MCl_4$ (M = Ti, Zr, Hf, and Rf). Experimental values are shown with *open triangles* connected by *dashed-dotted lines* (Reproduced with permission from Ref. [64]. Copyright 2014 American Institute of Physics)

(M = Ti, Zr, Hf, and Rf) [64, 65]. Results are shown in Table 4 for $MCl_4$. The trend in the formation of the tetrachlorides from the oxychlorides, formed in the oxygen atmosphere ahead of the pure halides, was found to be Zr < Hf < Rf. This means that if the pure chlorides of Zr and Hf exist under experimental conditions, $RfCl_4$ should also be stable.

Trends in $R_e$ and $\alpha$ of $MCl_4$ in the group, as well as the action of relativistic effects on them, are shown in Fig. 11. Relativistic effects are found to be responsible for the bond contraction in $HfCl_4$ and for even a larger bond contraction in $RfCl_4$, so that $\alpha(RfCl_4)$ is almost equal to $\alpha(TiCl_4)$.

For the long-range interaction of the $MCl_4$ (M = Zr, Hf, and Rf) molecules with a quartz surface, $\Delta H_{ads}$ were predicted with the use of the calculated molecular properties (Table 4) and Eq. (10). The obtained enthalpies (Table 4) show that volatility of the chlorides should increase smoothly in group 4: Zr < Hf < Rf. Thus,

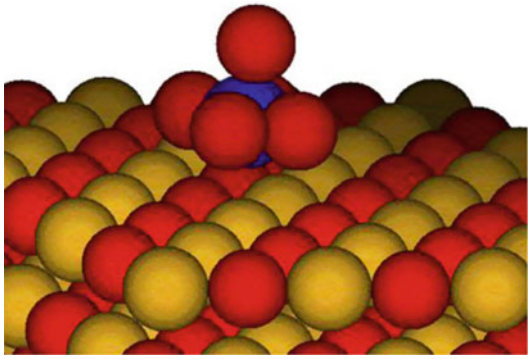

**Fig. 12** The $ML_6^-$ (M = Nb, Ta, and Db) complex formed on the KL (L = Cl, Br) surface (Reproduced with permission from Ref. [66]. Copyright 2012 American Institute of Physics)

$RfCl_4$ should be the most volatile species due to the relativistically decreased $\alpha$. (Nonrelativistically, $RfCl_4$ would have been less volatile than its homologs.) This trend is also in line with $\Delta H_{sub}(ZrCl_4) > \Delta H_{sub}(HfCl_4)$ [59]. For the formation of the $MCl_6^{2-}$ and $MOCl_4^{2-}$ complexes on a chlorinated quartz surface, the calculated energies of the complex formation reactions have given the following smooth trends in volatility: Zr > Hf > Rf and Zr < Hf < Rf, respectively [65]. The trend observed experimentally is, however, reversed, Zr < Hf > Rf, which cannot find its theoretical explanation from the molecular calculations and the assumed adsorption scenarios.

**Group 5**. Similarly to group 4, unusual reversed trends in volatility were also observed for group-5 halides: $NbCl_5 \approx DbCl_5 > TaCl_5$, $NbBr_5 > TaBr_5 > DbBr_5$, and $NbBr_5 \approx DbBr_5 > TaBr_5$ (see [5] for references). To find a reason for that, calculations for $ML_5$, $MOL_3$ (L = Cl and Br), and complexes $ML_6$ and $MCl_5Br$ (M = Nb, Ta, and Db) that can be formed on a halogenated quartz surface (Fig. 12) were performed using the 4c-DFT method [66].

Results of the calculations reveal a smooth change in properties of the compounds, as well as in their $E_{ads}$ on different surfaces, similarly to the group-4 (oxy)halides, but not the reversed trend observed experimentally.

The difference between the theoretical [64–66] and experimental [5] trends in volatility of group-4 and group-5 halides has not yet found its explanation. Detailed calculations of the interaction of the molecule with the adsorbent are not an easy task as modifications of the surface by the reactive agents occur and the structure of real surfaces is very hard to integrate into the model calculations. This work may, therefore, be prolonged, provided additional studies of surfaces and processes follow from the experimental side, as well as theoretical methods for molecular adsorption receive further development.

**Group 6**. In group 6, the most stable gas-phase oxychlorides are $MoO_2Cl_2$ and $WO_2Cl_2$. Stability and volatility of $SgO_2Cl_2$ were, therefore, to be investigated using isothermal phase-phase chromatography technique with a quartz column [67]. The 4c Dirac-Slater discrete variation (DS-DV) [68] and RECP [69] calculations for $MO_2Cl_2$ (M = Mo, W, and Sg) have found $SgO_2Cl_2$ to be also stable. However, its

**Table 5** Correlation and SO effects on the electronic density distribution ($Q_M$ and OP); dipole moments, $\mu$ (in D); and atomization energies, $D_e$ (in eV), of $MO_2Cl_2$ (M = W and Sg)

| | Molecule | RECP | | DFT |
|---|---|---|---|---|
| | | HF(AREP)[a] | SO-CCSD(T)[b] | DS-DV[c] |
| $Q_M$ | $WO_2Cl_2$ | 2.18 | 1.71 | 1.08 |
| | $SgO_2Cl_2$ | 1.94 | 1.52 | 0.97 |
| OP | $WO_2Cl_2$ | 2.14 | 2.03 | 2.23 |
| | $SgO_2Cl_2$ | 2.72 | 2.55 | 2.34 |
| $\mu$ | $WO_2Cl_2$ | 1.80 | 1.51 | 1.35 |
| | $SgO_2Cl_2$ | 2.64 | 2.39 | 1.83 |
| $D_e$ | $WO_2Cl_2$ | 11.7 | 22.2 | 23.8 |
| | $SgO_2Cl_2$ | 14.2 | 21.0(22.5[d]) | 21.8 |

[a]Average relativistic, i.e., without SO and correlation [69]
[b]With SO effects and correlation [69]
[c]Fully relativistic [68]
[d]Without SO effect

$D_e$ is somewhat smaller than $D_e(WO_2Cl_2)$ due to the SO effects (see Table 5). The following trend in volatility was predicted from the DFT calculated molecular properties (Table 5): $MoO_2Cl_2 > WO_2Cl_2 > SgO_2Cl_2$ [68]. The reason for this trend is increasing dipole moments in this row of molecules causing their stronger interaction with the surface. The experiments [67] have, indeed, demonstrated a decrease in volatility of the group-6 oxychlorides (see [5]), in good agreement with the predictions [68]. Thus, no unexpected behavior was observed in group 6 for Sg.

A search for a new class of volatile species suitable for gas-phase chromatography studies resulted in an idea to synthesize carbonyl complexes of the heaviest elements. Carbonyls proved to be also ideal for the transport of short-lived isotopes of the heaviest elements. Group-6 carbonyls including those of Sg were to be studied first using thermochromatography with a quartz column having a negative temperature gradient [70]. In turn, electronic structures of $M(CO)_6$ (M = Cr, Mo, W, and Sg) were calculated using the CCSD RECPs and 4c-DFT methods [71,72], with the latter work being devoted to predictions of their volatility. Since the nature of the molecule-surface interaction should be dispersive, $\Delta H_{ads}$ of Sg and of Mo carbonyls were predicted using Eq. (10) and the calculated molecular properties (Table 6) [72] with respect to the measured $-\Delta H_{ads}$ of $W(CO)_6$ of $46.5 \pm 2.5$ kJ/mol [70]. Results are shown in Table 6 and Fig. 13.

The obtained $\Delta H_{ads}$ of the Sg carbonyl turned out to be almost equal to $\Delta H_{ads}$ of $W(CO)_6$ due to the cancelling effects between its larger $\alpha$, though relativistically decreased, and its larger size ($x$ in Eq. 10). Experimental results [70] confirmed the theoretical predictions [72] showing an almost equal volatility of the W and Sg carbonyls (Table 6). Thus, Sg again proved to be an ordinary member of the group-6 elements.

**Group 7**. Group-7 elements Tc and Re form stable and volatile oxychlorides, $MO_3Cl$. Volatility of the Bh oxychloride, which should be formed by analogy with the lighter homologs, was to be studied using gas-phase isothermal chromatography

**Table 6** Ionization potentials, IPs (in eV); average dipole polarizabilities, $<\alpha>$ (in a.u.); interatomic distances, $R_e$ (in Å); and adsorption enthalpies, $-\Delta H^{\circ}_{ads}$ (in kJ/mol), of $M(CO)_6$, where M = Mo, W, and Sg, on quartz

| Molecule | Method | $R_e$(M-C)/$R_e$(C-O) | IP | $\alpha$ | $\Delta H^{\circ a}_{ads}$ | $\Delta H^{\circ b}_{ads}$ |
|---|---|---|---|---|---|---|
| $Mo(CO)_6$ | 4c-DFT | 2.063/1.145 | 9.00 | 156.4 | 48.1 ± 2.5 | 50 ± 2 |
| $W(CO)_6$ | 4c-DFT | 2.058/1.148 | 8.93 | 151.5 | 46.5 ± 2.5[c] | 49 ± 2 |
| $Sg(CO)_6$ | 4c-DFT | 2.123/1.154 | 8.63 | 159.4 | 46.2 ± 2.5 | 50 ± 4 |
| | RECP CC | 2.112/1.150[d] | | | | |

[a]Theory [72]
[b]Experiment [70]
[c]An experimental value taken as a reference point
[d]Theory [71]

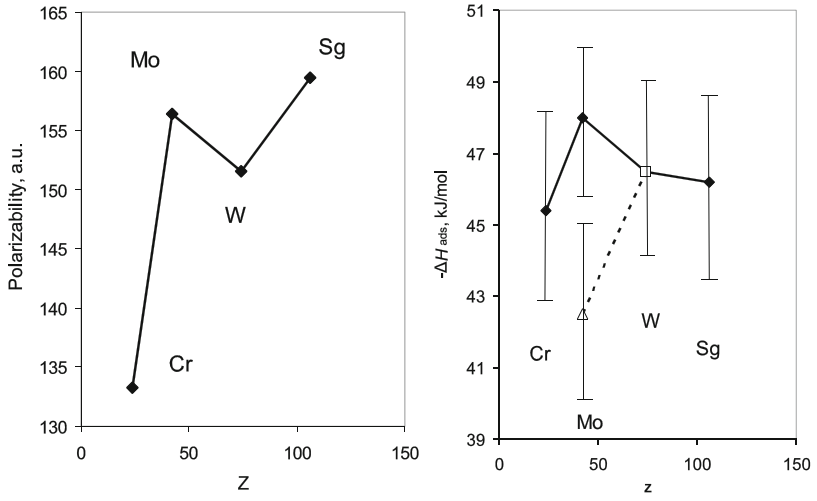


**Fig. 13** Calculated (*solid lines*) polarizabilities and adsorption enthalpies of $M(CO)_6$ (M = Cr, Mo, W, and Sg) on quartz [72]. The points (*open symbols*) for Mo and W are results of two different experiments [70] (Reproduced with permission from Ref. [72]. Copyright 2013 American Institute of Physics)

with a quartz column [73]. To predict an outcome of these experiments, energy contributions to the total molecule-surface interaction energy $E(x)$ for molecules having nonzero dipole moments were determined for $MO_3Cl$ (M = Tc and Bh) with respect to $E(x)$ of $ReO_3Cl$ using a model of long-range interactions [74] (Table 7). The resulting $-\Delta H_{ads}(BhO_3Cl)$ of 78.5 kJ/mol and $-\Delta H_{ads}(TcO_3Cl)$ of 48.2 kJ/mol turned out to be in very good agreement with the experimental $-\Delta H_{ads}(BhO_3Cl)$ of 75 kJ/mol and $-\Delta H_{ads}(TcO_3Cl)$ of 51 kJ/mol establishing the following trend in volatility: $TcO_3Cl > ReO_3Cl > BhO_3Cl$ (see Fig. 14, where the $BhO_3Cl$ yield curve is at the highest temperatures). Increasing dipole moments $\mu$ of $MOCl_3$ in the group were shown to be responsible for this decreasing trend.

**Table 7** Contributions to the interaction energy $E(x)$ of the $MO_3Cl$ molecules (M = Tc, Re, and Bh) with the chlorinated surface [$Q(Cl) = -0.4$] (From [74])

| Molecule | $\mu Qe$ | $\alpha Qe$ | $\alpha\alpha$(Cl) |
|---|---|---|---|
| | $E10^{16}$ $x^2$, eV cm$^2$ | $E10^{32}$ $x^4$, eV cm$^3$ | $E10^{48}$ $x^6$, eV cm$^6$ |
| $TcO_3Cl$ | 2.23 | 5.69 | 379.1 |
| $ReO_3Cl$ | 3.10 | 6.81 | 460.7 |
| $BhO_3Cl$ | 4.67 | 8.63 | 591.2 |

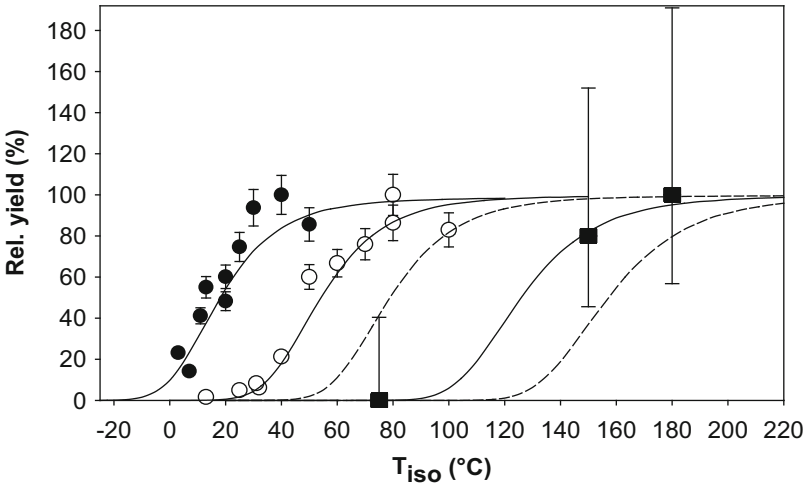


**Fig. 14** The relative yields of $TcO_3Cl$ (*filled black circles*), $ReO_3Cl$ (*open circles*), and $BhO_3Cl$ (*filled black squares*) as a function of the isothermal temperatures, $T_{iso}$, in isothermal gas-phase experiments (Reproduced with permission from Ref. [73]. Copyright 2000 Nature Publishing Group)

**Group 8**. Group-8 elements Ru and Os are known to form stable and volatile tetroxides, $MO_4$. Volatility of $HsO_4$ was, therefore, of interest. It was to be studied with respect to that of $OsO_4$ using gas-phase thermochromatography with a quartz column [75]. Accordingly, the 4c-DFT calculations were performed for $MO_4$ (M = Ru, Os, and Hs) [76]. Results are given in Table 8 and Fig. 15 showing excellent agreement of IP, $\alpha$, and $R_e$ with experimental data for $RuO_4$ and $OsO_4$. The high accuracy of the calculations was achieved by using extremely large basis sets.

The measured relatively low $-\Delta H_{ads}(OsO_4)$ on quartz was indicative of the van der Waals type of adsorption [75]. Taking this into account, $-\Delta H_{ads}(HsO_4)$ of only 6 kJ/mol larger than $-\Delta H_{ads}(OsO_4)$ was calculated using Eq. (10) and the computed molecular properties (Table 8) [76], in excellent agreement with the experimental $-\Delta H_{ads}(HsO_4)$ and the observed $T_{ads}(HsO_4) > T_{ads}(OsO_4)$ [75] (Fig. 16). The obtained $\Delta H_{ads}(MO_4)$ show a reversal of the trend in group 8, the same as $\alpha$ and IP do, which is stipulated by the trend reversal in the energies of the $(n-1)$d AOs (see Fig. 1b in [76]). This example shows that for very similar species, a particularly

**Table 8** Ionization potentials, IPs (in eV); polarizabilities, $\alpha$ (in a.u.); bond lengths, $R_e$ (in Å); vibrational frequencies, $\nu_e$, of the M-O bond (in $cm^{-1}$); and adsorption enthalpies, $-\Delta H^\circ_{ads}$ (in kJ/mol), on quartz for $MO_4$ (M = Ru, Os, and Hs)

| Property | Method[a] | $RuO_4$ | $OsO_4$ | $HsO_4$ |
|---|---|---|---|---|
| IP | Calc. | 12.21 | 12.35 | 12.29 |
| | Exp. | 12.19 | 12.35 | – |
| $\alpha$ | Calc. | 58.07 | 55.38 | 65.99 |
| | Exp. | 58.64 | 55.13 | – |
| $R_e$ | Calc. | 1.712 | 1.719 | 1.779 |
| | Exp. | 1.706 | 1.711 | – |
| $\nu_e$ | Calc. | 851 | 900 | 989 |
| | Exp. | 880 | 965 | – |
| $\Delta H_{ads}$ | Calc. | 41.0 ± 1 | 39.0 ± 1 | 45.4 ± 1 |
| | Exp.[b] | | 39.0 ± 1 | 46.0 ± 2 |

[a]Calculations are from [76]; see also references for experimental values there
[b]Ref. [75]

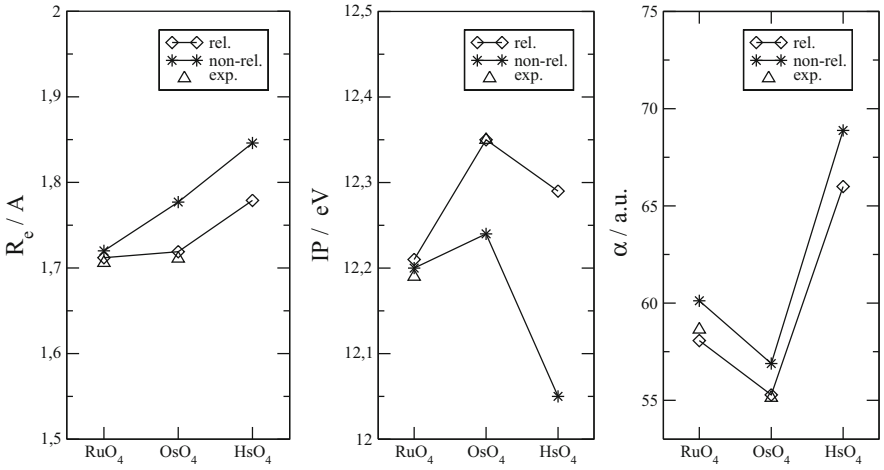


**Fig. 15** Relativistic (rel.) and nonrelativistic (nonrel.) bond lengths, $R_e$; ionization potentials, IPs; and polarizabilities, $\alpha$, of $MO_4$ (M = Ru, Os, and Hs) (Reproduced with permission from Ref. [76]. Copyright 2008 American Physical Society)

high accuracy of the calculations is required in order to "detect" tiny differences in their molecular and adsorption properties. A linear extrapolation of $\Delta H_{ads}$ in group 8 proved to be unreliable.

Relativistic effects were shown to have no influence on the trends in the molecular properties and $\Delta H_{ads}(MO_4)$ in group 8 (Fig. 15), because of identical trends in the energies and $R_{max}$ of the charge density of the relativistic and nonrelativistic $(n-1)$d AOs responsible for bonding.

**Group 9, 10, and 11**. Mt and Ds have received little attention so far, because very short half-lives of their isotopes are not suitable for experimental investigations.

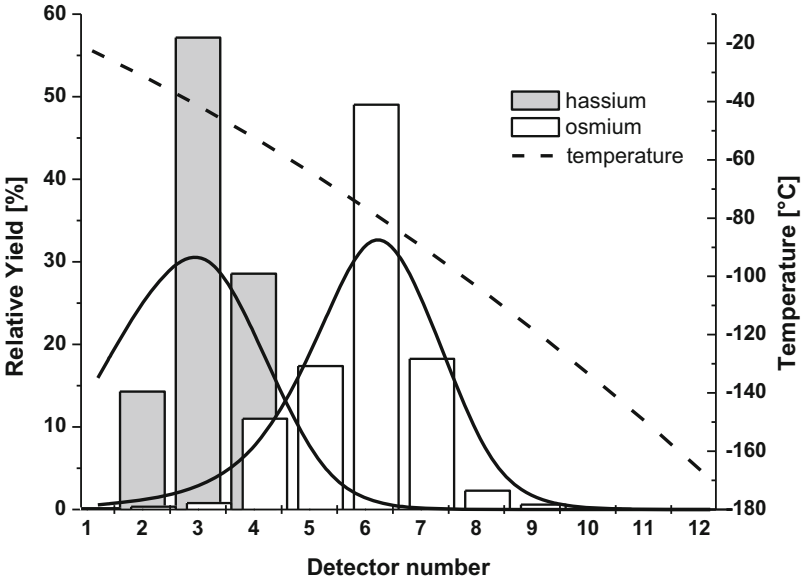


**Fig. 16** Observed adsorption behavior of $OsO_4$ and $HsO_4$ in the gas-phase thermochromatography experiments (Reproduced with permission from Ref. [75]. Copyright 2002 Nature Publishing Group)

A few theoretical studies deal with $DsF_6$, DsX (X = H, C, and CO) of $DsH_3$ (see [9] for references).

Chemistry of Rg was, on the contrary, of much theoretical interest: unusual properties of its compounds were anticipated due to the strongest relativistic stabilization of the 7s AO in group 11. Particularly, the electronic structure of RgH, a sort of a test molecule like AuH, was of interest in probing the accuracy of various methods in predicting the trend from $R_e$(AuH) to $R_e$(RgH) (see Table 13 of [9]). The 4c-DFT and DHF CCSD(T) results were proven to be most accurate. The SR effects were shown to double $D_e$(RgH), though the SO effects on the Rg atom diminish it by 0.7 eV. The trend to an increase from $D_e$(AgH) to $D_e$(AuH) turns, therefore, out to be reversed from $D_e$(AuH) to $D_e$(RgH).

**Group 12**. Group-12 elements have a $(n-1)d^{10}ns^2$ closed-shell ground state. With increasing relativistic effects in this group, the elements become more inert. Thus, Hg is known to be a liquid. For Cn, the maximum of the relativistic stabilization of the 7s AO in the group (Fig. 2), as well as in the 7th row of the periodic table, was a reason to believe it to be noble gas-like: In 1975, Pitzer suggested that the very high valence-state excitation energy $6d^{10}7s^2 \rightarrow 6d^{10}7s7p_{1/2}$ of 8.6 eV will not be compensated by the energy gain of the chemical bond formation [77].

The idea of Cn having noble gas properties was tested by gas-phase thermochromatography experiments allowing for comparison of its volatility with that of Hg,

a lighter homologous d element, and Rn, an inert gas [78]. Gold was chosen as a surface of detectors of a chromatography column: it strongly adsorbs Hg, while very weakly Rn. The questions to the electronic structure theory were, therefore: Is Cn metallic in the solid state, or is it more like a solid noble gas? How volatile and reactive toward gold is the Cn atom in comparison with Hg and Rn?

*Homonuclear dimers.* Bonding in the solid state, i.e., cohesive energy, $E_{\mathrm{coh}}$, of an element can be described in the first approximation by bonding in its homonuclear dimer, $M_2$. $D_e(Cn_2)$ had, therefore, to be accurately calculated. Moreover, $Hg_2$ and $Cn_2$ were of interest for theory in probing the accuracy of various methods in treating closed-shell interactions. Accordingly, the electronic structures of $Hg_2$ and $Cn_2$ were calculated using a variety of methods, such as X2C CCSD(T) [79], 4c-BDF, ECP CCSD(T), QR PP CCSD(T) [54], 4c-BDF [80], and 4c-DFT [81]. Some results are shown in Table 9 and Fig. 17. A more complete table is given in [9].

As expected, the DFT underestimates $D_e(M_2)$ (M = Hg and Cn) [54, 81], but nicely reproduces the trend to an increase in it of 0.04 eV from $Hg_2$ to $Cn_2$, also shown by the CCSD(T) calculations [54, 79] (Fig. 17). As the nature of this interaction is predominantly dispersive, such an increase is due to a smaller M-M distance caused by the smaller $R_{\mathrm{max}}$ of the 7s(Cn) AO in comparison with $R_{\mathrm{max}}$ of the 6s(Hg) AO. This is a first indication that the cohesive energy, $E_{\mathrm{coh}} \approx \Delta H_{\mathrm{sub}}$, of bulk Cn should be larger than $E_{\mathrm{coh}}$(Hg).

*Solid state.* LDA DFT (nonrelativistic, scalar relativistic, SR, and 4c relativistic) band structure calculations were performed on the Cn solid state [83]. The results have shown that Cn prefers the *hcp* structure (as that of Zn and Cd) in the difference to Hg (*fcc*). Thus, it should differ from its lighter homolog Hg on a structural level and resemble the solid-state noble gases. A cohesive energy of 1.13 eV was obtained for Cn at the SR level of theory, which is larger than that of Hg (0.64 eV) and is an order of magnitude larger than those of the solid noble gases. It was concluded that Cn is not a metal, but rather a semiconductor with a band gap of at least 0.2 eV. In this sense, Cn resembles the group-12 metals more closely than it does the noble gases. This result is consistent with the larger $D_e(Cn_2)$ with respect to $D_e(Hg_2)$.

**Table 9** Bond lengths, $R_e$ (in Å), and dissociation energies, $D_e$ (in eV), of $Hg_2$, $Cn_2$, and $Fl_2$

| | $Hg_2$ | | $Cn_2$ | | $Fl_2$ | | |
|---|---|---|---|---|---|---|---|
| Method | $R_e$ | $D_e$ | $R_e$ | $D_e$ | $R_e$ | $D_e$ | Ref. |
| X2C CCSD(T) | 3.744 | 0.050 | 3.461 | 0.084 | 3.547 | 0.117 | [79] |
| 4c-BDF (PBE) | 3.904 | 0.025 | 3.363 | 0.075 | 3.490 | 0.12 | [54,80] |
| RECP CCSD(T) | 3.73 | 0.049 | 3.320 | 0.095 | 3.730 | 0.07 | [54,80] |
| QR PP CCSD(T) | 3.769 | 0.044 | 3.386 | 0.097 | – | – | [54] |
| 4c-DFT (B88/P86) | 3.63 | 0.010 | 3.450 | 0.050 | 3.490 | 0.13 | [81,82] |
| Exp.[a] | 3.63 | 0.043 | – | – | – | – | |

[a]See the original publications for references

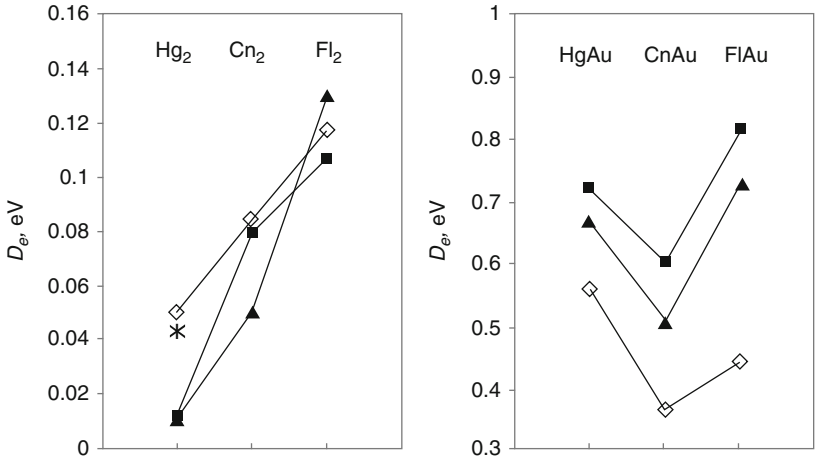


**Fig. 17** Dissociation energies of $M_2$ and MAu, where M = Hg, Cn, and Fl: the (2c) BSS CCSD(T) values are *open rhomboids*, the (2c) BSS DFT (B88/P86) data are *filled squares* [79], and the 4c-DFT (B88/P86) data are *filled triangles* [81, 82]. The experimental $D_e(Hg_2)$ is shown with a star

Thus, the case of group-12 elements shows that the relativistic calculations are indispensable in order to predict the right trend in volatility, Cn < Hg, or $\Delta H_{sub}$(Cn) > $\Delta H_{sub}$(Hg), while an extrapolation of $\Delta H_{sub}$ in group 12 gives 22.2 kJ/mol for Cn, which is the lowest in group 12.

*Interaction with metals.* In order to predict volatility of Hg and Cn as adsorption enthalpy on gold, $\Delta H_{ads}{}^{Au}$(M) (and other noble metals), measured in the gas-phase experiments [78], 4c-DFT calculations were performed for MM′ (M = Hg, Cn; M′ = Ag, Au, Pt, Pd, and Cu) [84] and M-$Au_n$ systems, where $Au_n$ ($n = 1$ through 120) are clusters simulating a gold surface [85, 86]. It was shown that Cn interacts rather well with the noble metals. In CnAu, the $\sigma$-bond formation takes place between the doubly occupied 7s(Cn) AO and the singly occupied 6s(Au) AO (Fig. 18). $D_e$(CnAu) is, however, smaller than $D_e$(HgAu) due to the more stabilized 7s(Cn) AO than 6s(Hg) AO. Among different metals M, bonding of Cn with Pd should be the strongest, while with Ag the weakest [84].

Since the structure of the real gold surface is unknown, two types of ideal surfaces were considered: Au(100) and Au(111) [85, 86]. For the Au(111) surface that is more realistic, the convergence in $E_b$(M-$Au_n$) (M = Hg and Cn) with the cluster size was reached for $n = 95$ for the top, $n = 94$ for the bridge, and $n = 120$ for the hollow-1 and $n = 107$ for the hollow-2 positions. For Hg, the bridge position was found to be preferential for both types of surfaces, while for Cn, the hollow 2. $E_b$(Cn-$Au_n$) of 0.46 eV on the Au(111) surface was given then as a final prediction [86] (Table 10 and Fig. 19).

The measurements of volatility of Cn have shown that Cn adsorbs in the chromatography column on gold at $T_{ads}$ around −20 °C, which is much lower than

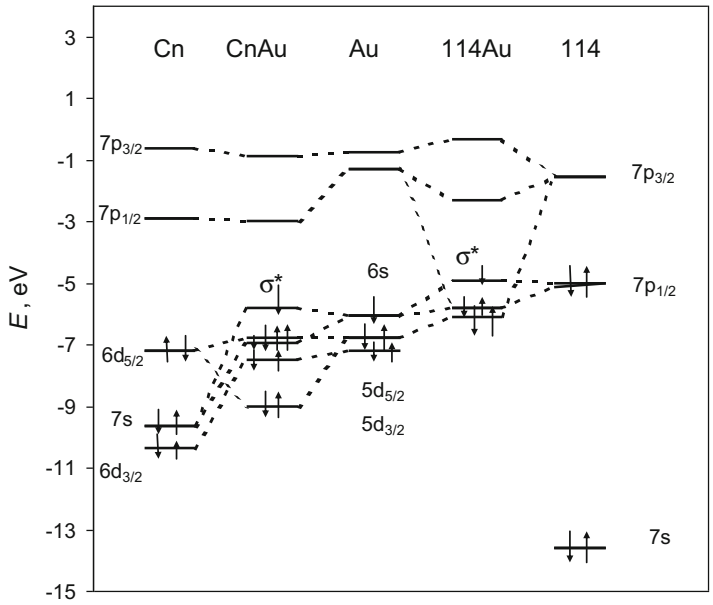


**Fig. 18** Chemical bond formation in CnAu and FlAu (Reproduced with permission from Ref. [11]. Copyright 2011 Oldenbourg Wissenschaftsverlag GmbH)

**Table 10** The Cn-Au$_n$ and Fl-Au$_n$ binding energies and $-\Delta H^\circ_{ads}$(M) on gold (M = Cn and Fl) (in eV)[a]

| Method | n/surface | Cn | Fl | Ref. |
|---|---|---|---|---|
| 4c-DFT | 1 | 0.51 | 0.73 | [86] |
| 2c-DFT | 1 | 0.47 | 0.72 | [87] |
| SO DFT | 3 | 0.47 | 0.77 | [87] |
| 2c-DFT | $26^{br}$/Au(100) | 0.33 | 0.55 | [86] |
| 2c-DFT | $37^{holl-2}$/Au(111) | – | 0.49 | [88] |
| 4c-DFT | $95^{top}$/Au(111) | 0.30 | 0.47 | [86] |
| 4c-DFT | $94^{br}$/Au(111) | 0.42 | **0.71** | [86] |
| 4c-DFT | $107^{holl-2}$/Au(111) | **0.46** | 0.59 | [86] |
| Exp. | $-\Delta H^\circ_{ads}$(M)/Au[b] | $0.54^{+0.2}_{-0.04}$ | $0.34^{+0.5}_{-0.1}$ | [78, 89] |
| | | | $> 0.50$ | [90] |

[a]Most stable states are in bold
[b]The structure of the gold surface is unknown

$T_{ads}$ of Hg (Hg adsorbs right at the beginning of the column with 35 °C), but higher than $T_{ads}$(Rn) of −180 °C [78]. The obtained $-\Delta H_{ads}{}^{Au}$(Cn) $= 0.54^{+0.2}_{-0.01}$ eV ($52^{+20}_{-4}$ kJ/mol) turned out to be in good agreement with the theoretical value [86]. Such a relatively high $-\Delta H_{ads}{}^{Au}$(Cn) was evident of the metal-metal bond formation, a behavior typical of group-12 lighter homologs.

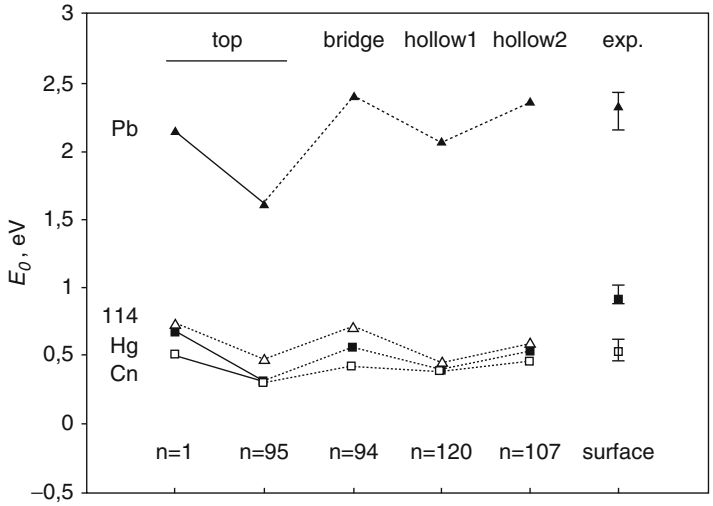


**Fig. 19** The 4c-DFT calculated binding energies of Pb, Hg, Cn, and Fl with $Au_n$ simulating a Au(111) surface and experimental $-\Delta H_{ads}$ of Pb, Hg, and Cn on gold (Reproduced with permission from Ref. [86]. Copyright 2009 American Institute of Physics)

Works on the RECP and 2c-DFT calculations for Hg and Cn interacting with different gold clusters arrived at the same conclusion: $E_b$(Cn-$Au_n$) is about 0.2 eV smaller than $E_b$(Hg-$Au_n$) (Table 10) [87]. (The data for Fl$Au_n$ are also given in Table 10 [88–90], but discussed below.) In [47], the influence of relativistic effects on $E_b$(M-$Au_n$) (M = Hg and Cn) was investigated. Relativistic effects were shown to increase $E_b$(M-$Au_n$) of both the Hg- and Cn-containing species and to be responsible for $E_b$(Hg-$Au_n$) > $E_b$(Cn-$Au_n$).

In summary, both the theoretical and experimental studies show that Cn forms a rather strong bond, however weaker than that of Hg, with metals. Thus, it behaves like a d element upon adsorption, but not like an inert gas. In this way, its position in group 12 of the periodic table has been confirmed. The obtained - $\Delta H_{ads}{}^{Au}$(Cn) < $-\Delta H_{ads}{}^{Au}$(Hg) *do not correlate* with $\Delta H_{sub}$(Cn) > $\Delta H_{sub}$(Hg) due to the different types of bonding in these two cases. The example of group-12 elements shows how important are theoretical calculations in order to distinguish between the nature of the studied processes and trends in the group.

Some other compounds of Cn, hydrides, and fluorides were also considered theoretically. A review of those works can be found elsewhere [5, 8–11].

**Groups 13 through 18**. In the 7p elements, the $7s^2$ electrons are bound more tightly than the $6s^2$ ones in the 6p homologs, so that they do not take part in the chemical bond formation. Also, a large SO splitting of the 7p shell into the *nlj* subshells should result in differences in the chemical bonding in comparison with the homologs having (almost) a complete *nl* shell. Thus, these elements are expected

to be more volatile than their lighter homologs, as their $\Delta H_{sub}$ obtained via linear extrapolations in the groups indicate [91].

Experimentally, volatility of the 7p elements at the beginning of the series, i.e., those with sufficiently long half-lives, is supposed to be studied using gas-phase chromatography techniques with gold- or $SiO_2$-plated detectors. First results for adsorption on gold with the use of thermochromatography have been published for $^{289}$Fl ($t_{1/2} = 2.1$ s) and $^{288}$Fl ($t_{1/2} = 0.7$ s) [89, 90]. The next element to be studied is $^{284}113$ with $t_{1/2} \approx 0.9$ s.

*Homonuclear dimers.* Keeping again in mind that bonding in $M_2$ is related to bonding in the solid state, $D_e(M_2)$ were calculated for the entire series of the 6p and 7p elements using the 4c-DFT method [92, 93]. (A few dimers were also calculated in [80]). All the dimers of group-13 through group-17 7p elements were shown to be, indeed, weaker bound than their 6p homologs, with the difference in $D_e(M_2)$ between them decreasing with the group number and a final reversal of the trend in group 18 (Fig. 20). The reason for that is very large SO effects on the 7p AOs preventing them from making a full $\sigma$-bond: in $(113)_2$ and $Fl_2$, bonding is preferentially made by the $7p_{1/2}$ AOs, while in the heavier elements, mainly by the $7p_{3/2}$AOs.

An interesting observation was the shift of the $D_e(M_2)$ maximum in the seventh row toward group 16 with respect to group 15 in the sixth and upper rows (Fig. 20). This is also a strong manifestation of the relativistic effects. As a result of the stabilization of the $7p_{1/2}$ AOs, the system of the highest bonding-antibonding MOs in $M_2$ consists of only four MOs composed of the $7p_{3/2}$ AOs, so that the half-filled shell (with four electrons) falls on $(116)_2$. In contrast, the $6p_{1/2}$ and $6p_{3/2}$ AOs are not so well separated energetically from each other and form a set of six highest bonding-antibonding MOs, so that the half-filled shell (with six electrons) falls on $Bi_2$ (see Fig. 4 in [92]).

*Flerovium.* Due to the very large SO splitting of the 7p AOs (Fig. 2), Fl has a quasi-closed-shell ground state, $7s^27p_{1/2}^2$. The argument of Pitzer, similar to that used for Cn, which due to the $7p_{1/2}$(Fl) AO stabilization, the $7p_{1/2}^2 \rightarrow 7p^2$ promotion energy to the metal valence state will not be compensated by the metal bond formation, led to the conclusion that this element should be a relatively inert gas or a volatile liquid bound by van der Waals forces [77]. To test this assumption at the MO level of theory, electronic structures of $Fl_2$ (and $Pb_2$ for comparison) were calculated using DFT and CC methods [80, 92]. The calculations agree on the fact that bonding in $Fl_2$ is stronger than a typical van der Waals one. It is stronger than that in $Cn_2$, but much weaker than that in $Pb_2$ (Table 9 and Fig. 20). A Mulliken population analysis indicates that both the $7p_{1/2}$ and $7p_{3/2}$ AOs of Fl take part in the chemical bond formation. SO effects were shown to decrease $D_e$, but increase $R_e$ in both $Pb_2$ and $Fl_2$ [80]. The DFT results [81, 82] perfectly reproduce the trend to an increase in $D_e$ from $Hg_2$ to $Cn_2$ and further to $Fl_2$ in agreement with the CC calculations [79], where dispersion interactions are more fundamentally taken into account (Table 9 and Fig. 17). Also, the 4c-DFT and CCSD(T) $D_e(Fl_2)$ nicely agree with each other

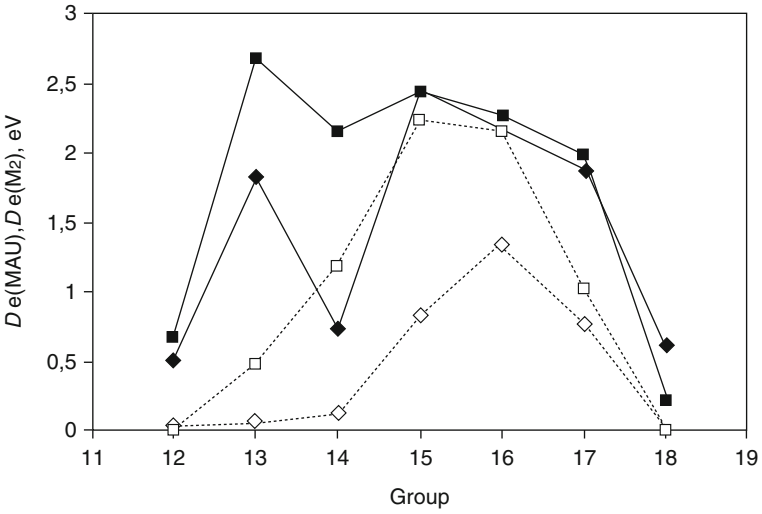


**Fig. 20** Calculated dissociation energies of MAu and $M_2$ (M are elements Hg/Cn through Rn/118). *Filled* and *open squares* are $D_e$(MAu) and $D_e(M_2)$ of the 6p elements, respectively, while *filled* and *open rhomboids* are $D_e$(MAu) and $D_e(M_2)$ of the 7p elements, respectively (Reprinted with permission from Ref. [93]. Copyright 2010 American Institute of Physics)

confirming that the Fl-Fl interactions are of no van der Waals nature. This is a clear indication that the Fl-Fl bonding should be stronger than the Cn-Cn one, also in the bulk.

In the difference to the other 7p elements, the bond in $(118)_2$ should be stronger than that of the lighter group-18 homologs due to its largest $\alpha(118)$ in the group [92].

*Sublimation enthalpies.* The $D_e(M_2)$ of the np elements were shown [92] to nicely correlate with $\Delta H_{\rm sub} = \Delta H^{\circ}_f(g)$ of bulk of these elements [59]. Obtained on the basis of this correlation, $\Delta H_{\rm sub}$ of the 7p elements are smaller than those of the lighter homologs and agree rather well with $\Delta H_{\rm sub}$ predicted via a linear extrapolation in groups 13–17 [91]. Thus, elements 113 through 117 should, indeed, be more volatile than their lighter homologs.

In [94], $E_{\rm coh}$(Fl) of 0.5 eV was predicted from SR and SO DFT (PW91) periodic calculations. The resulting value is in good agreement with $\Delta H_{\rm sub}$ obtained from a correlation with $D_e(M_2)$ in group 14 [92]. SO effects were shown to lower $E_{\rm coh}$ and to lead to structural phase transitions for the solid Fl having the *hcp* structure in contrast to the *fcc* one for Pb.

*Interaction with metals and adsorption on gold.* In order to predict $\Delta H_{\rm ads}$ of the 7p elements on gold, 4c-DFT calculations for the MAu dimers were performed in [93]. Obtained $D_e$(MAu) are shown in Fig. 20 in comparison with $D_e(M_2)$. One can see that in group 13 and 14, $D_e$(MAu) of the 7p elements are smaller than $D_e$ of the 6p homologs, which is explained by the relativistic stabilization of the $7p_{1/2}$ AOs. On

the contrary, in groups 15 through 17, they are about the same. This is in contrast to the trends in $D_e(M_2)$, where $D_e(Bi_2) >> D_e[(115)_2]$, $D_e(Po_2) >> D_e[(116)_2]$, and $D_e(At_2) > D_e[(117)_2]$. The relatively strong M-Au bonding of elements 115 through 117 with gold is explained by the relativistic destabilization of the $7p_{3/2}$(M) AO fitting nicely to the 6s(Au) AO, thus making – together with the $7p_{1/2}$(M) AO – a full $\sigma$-bond in the difference to $M_2$, where only the $7p_{3/2}$(M) AO are involved in bonding. In group 18, a reversal takes place, so that $D_e(118Au) > D_e(RnAu)$, in agreement with the trend in $D_e(M_2)$. This is due to the relativistically destabilized $7p_{3/2}(118)$ AO better fitting to the 5d and 6s AOs of Au than the $6p_{3/2}$(Rn) AOs.

The 4c-DFT calculations were also performed for group-14 intermetallic dimers MM', where M' are group-10 and group-11 elements [82]. The Fl-Pt bonding was found to be the strongest, while the Fl-Ag and Fl-Ni, the weakest.

Using $D_e$(MAu), $-\Delta H_{ads}$ of element 113 and Fl on gold of 159 and 92 kJ/mol, respectively, were estimated via a correlation between these quantities in groups 13 and 14 [93, 95]. In groups 15 through 17, no correlation is observed between these quantities, because $D_e$(M-Au) does not decrease linearly with Z, while $D_e$(M-M) does [93]. Thus, the case of the 7p elements with large SO effects shows that linear extrapolations of properties, such as $\Delta H_{ads}{}^{Au}$(M), from the lighter homologs in the groups might lead to erroneous predictions.

The 2c-DFT and 1c-CCSD(T) calculations were performed for $MAu_n$, where M = Tl and element 113 ($n = 1, 2, 3$, and 58) [96], with the gold clusters simulating Au(100) and Au(111) surfaces. The difference in $E_b$(M-$Au_n$) between Tl and element 113 was found to stay within $\pm$15 kJ/mol of 82 kJ/mol obtained for $D_e$(MAu) [93]. Thus, taking into account $-\Delta H_{ads}$(Tl) of 240 kJ/mol [97], $-\Delta H_{ads}$(113) can presently be given as 159 $\pm$ 15 kJ/mol.

Extended 4c-DFT calculations were also performed for M = Pb and Fl (along with Hg and Cn) interacting with large $Au_n$ clusters ($n = 1$ through 120) simulating the Au(111) surface [86]. Both Pb and Fl were found to prefer the bridge adsorption position, where the convergence in $E_b$(M-$Au_n$) with the cluster size was reached for $n = 94$ (Table 10 and Fig. 19). The calculated $E_b$ turned out to be in very good agreement with the experimental $-\Delta H_{ads}$ of Pb and Cn on gold [78] indicating that the Au(111) surface is obviously the proper one. Taking into account that Hg dissolves in gold, the trend in $-\Delta H_{ads}{}^{Au}$(M) was predicted as Cn < Fl < Hg $\ll$ Pb [86].

Particularly interesting is the comparison of Fl with Cn, both revealing relatively weak metal-surface interaction. Both the 4c-DFT [86, 93] and BSS CCSD(T) [79] calculations for the gold dimers, as well as for large metal-gold cluster systems [86–88], have shown Fl to be stronger bound with Au than Cn (Table 10 and Fig. 19). The reason for that is the following: in FlAu – even though both FlAu and CnAu are open-shell systems with one antibonding $\sigma^*$ electron – electron density is donated from the lying higher in energy $7p_{1/2}$(Fl) AO to the 6s(Au) AO, while in CnAu, some excitation energy is needed to transfer some electron density from the closed $7s^2$(Cn) shell to the 6s(Au) AO (Fig. 18).

In contrast to the theoretical predictions, the first thermochromatography experiment with three events of Fl has shown that it adsorbs on the surface of chro-

matography column with gold detectors at temperatures about those of Rn and $-\Delta H_{ads}{}^{Au}$(Fl) of 0.34 $^{+0.54}_{-0.11}$ eV has been given on their basis [89], smaller than $-\Delta H_{ads}{}^{Au}$(Cn) of 0.54 $^{+0.02}_{-0.04}$ eV (Table 10). Such a small $-\Delta H_{ads}{}^{Au}$(Fl) was interpreted as an indication of "the formation of a weak physisorption bond between atomic Fl and a gold surface." According to these results, Fl should have been chemically more inert than Cn. The second similar experiment on volatility of Fl, conducted at a lower background of interfering products, registered two events of this element adsorbed on gold at room temperature [90]. Such a relatively high $T_{ads}$ and estimated $-\Delta H_{ads}{}^{Au}$(Fl) > 48 kJ/mol support the theoretical conclusion that Fl should form a chemical bond with Au. Further experiments are underway to collect better statistics of the Fl events in order to have a more accurate $\Delta H_{ads}$(Fl).

*Other compounds.* Other than elements 114 and 118, elements 113 and 115 through 117 will not be stable in the gas phase in the elemental state. Thus, element 113 should form hydroxides in the presence of traces of water in the experimental setup. Relativistic 4c-DFT calculations have shown the 113-OH bond to be rather strong (2.42 eV), but weaker than the Tl-OH one (3.68 eV) [95]. Element 113 may then adsorb on gold in the form of the hydroxide. $-\Delta H_{ads}{}^{Au}$(113OH) is expected to be lower than $-\Delta H_{ads}{}^{Au}$(113).

There are numerous relativistic – DCB, RECP, and 4c-DFT – calculations of other compounds of group-13 elements, such as MX and $MX_3$ (X = H, F, Cl, Br, and I), or (113)(117). A very large bond contraction is found in 113X due to the $7p_{1/2}$(113) AO contraction, as in none of the other compounds (see [9] as a review). The electronic structures of FlX (X = F, Cl, Br, I, O, $O_2$) were calculated using the 2c-RECP CCSD(T), 2c-DFT SO ZORA, and 4c-BDF methods [80]. In contrast to $PbO_2$ ($D_e$ = 5.60 eV), $FlO_2$ ($D_e$ = 1.64 eV) was predicted to be thermodynamically unstable with respect to the decomposition into the metal atom and $O_2$.

Chemistry of elements 115, 116, and 117 received little attention so far. Chemistry of element 118, on the contrary, was of much theoretical interest. It should be unusual due to the huge SO effects (11.8 eV) preventing the $7p^2_{1/2}$ pair from the participation in the chemical bond. Thus, a different geometry of $118F_4(T_d)$ than that of $RnF_4$ ($D_{4h}$) was predicted due to availability of only $7p^4_{3/2}$ electrons of element 118 for bonding [98]. (See also [7–11] for reviews.)

*Summary.* Predicted trends in volatility of group-4 through group-8, group-12, and group-14 species in comparison with observations are given in Table 11. They show largely the synergy between theory and experiment. Observed unusual trends in volatility of group-4 and group-5 halides, as well as of Fl with respect to Cn, belong to the few unresolved cases that may require further research efforts.

**Elements 119 and 120**. Elements 119 and 120 are the next elements awaiting discovery. Their properties should be defined by the 8s and $8s^2$ ground-state configurations, respectively. Volatility of atoms of elements 119 and 120 might be studied in the long term using an advanced (vacuum) chromatography technique designed for extremely short, presumably sub-millisecond, half-lives of their isotopes.

**Table 11** Trends in volatility of group-4–8, group-12, and group-14 species

| Group | Volatile species | Theoretically predicted | Ref. | Experimentally observed | Ref.[a] |
|---|---|---|---|---|---|
| 4 | $ML_4$ (L = Cl, Br) | Zr < Hf < Rf | [64, 65] | Hf < Rf ≈ Zr | See [5] |
| 5 | $ML_5$(L = Cl, Br) | Nb < Ta < Db | [66] | Ta < Db ≈ Nb | See [5] |
| | $MOL_3$ (L = Cl, Br) | Nb > Ta > Db | [66] | Nb > Ta > Db | See [5] |
| 6 | $MO_2Cl_2$ | Mo > W > Sg | [68] | Mo > W > Sg | [67] |
| | $M(CO)_6$ | Mo ≈ W ≈ Sg | [72] | Mo ≈ W ≈ Sg | [70] |
| 7 | $MO_3Cl$ | Tc > Re > Bh | [74] | Tc > Re > Bh | [73] |
| 8 | $MO_4$ | Ru < Os > Hs | [76] | Os > Hs | [75] |
| 12 | M | Hg < Cn | [86] | Fl > Cn | [78, 89] |
| 14 | M | Fl < Cn | [86] | Fl ≤ Cn | [90] |

[a]For most experimental studies, see references in [5]

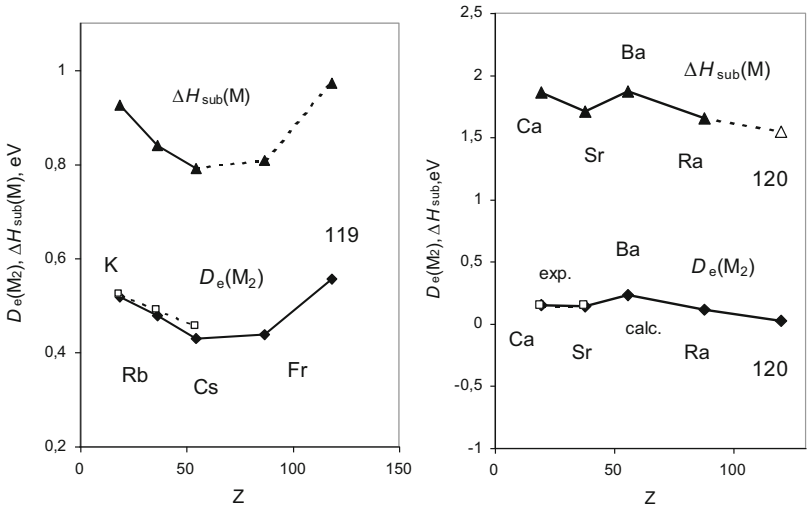


**Fig. 21** Dissociation energies, $D_e$, of group-1 and group-2 $M_2$ (*filled rhomboids* are 4c-DFT calculations, *open squares* – experiment), as well as sublimation enthalpies, $\Delta H_{sub}$(M) (*filled triangles* connected by solid lines are experiment, those connected by dashed lines – estimates) (Reproduced with permission from Refs. [99] and [100]. Copyright 2012 Elsevier and 2012 American Institute of Physics, respectively)

*Homonuclear dimers and sublimation enthalpies.* To estimate $\Delta H_{sub}$ of elements 119 and 120, the 4c-DFT calculations were performed for group-1 and group-2 homonuclear dimers [99, 100]. The obtained $D_e(M_2)$ show a reversal of trends at Cs in group 1 and at Ba in group 2, though in the opposite direction: an increase in group 1 from Cs on and a decrease in group 2 from Ba on (Fig. 21). The reason for these different trends is the different types of the M-M binding in these two cases: a covalent ns(M)-ns(M) one in group 1, while a van der Waals $ns^2$(M)-$ns^2$(M) one in group 2. Accordingly, $R_e(M_2)$ decreases in group 1 from Cs toward element 119, while it steadily increases in group 2.

A linear correlation between $D_e(M_2)$ and $\Delta H_{sub}(M)$ was established in these groups. On its basis, $\Delta H_{sub}$ of element 119 of 94 kJ/mol and of element 120 of 150 kJ/mol were obtained (Fig. 21) [99, 100]. According to these data, the element 119 metal should be as strongly bound as K, while the element 120 metal should be most weakly bound in group 2, though stronger than the element 119 one. A reversal of the M-M binding trends in these groups is a result of the $E$(ns) AO trend reversal from the 6th row on.

*Intermetallic dimers and adsorption on noble metals.* In order to predict $\Delta H_{ads}(M)$ of elements 119 and 120 on noble metals, electronic structures of MAu, where M are group-1 and group-2 elements, were calculated using the 4c-DFT method [99, 100]. The 2c-DFT calculations were also performed for the 120-$Au_n$ clusters [101]. Elements 119 and 120 were shown to strongly interact with gold though weaker than the homologs. The $D_e$(MAu) values reveal a reversal of the increasing trend at Cs and Ba in group 1 and 2, respectively (Fig. 22), in accordance with the trend reversal in $E$(ns) AO. They were also shown to correlate with the semiempirical $-\Delta H_{ads}(M)$ [102] of K through Cs and Ca through Ba on gold and other metals, respectively. On the basis of these correlations, $-\Delta H_{ads}$ of element 119 of 106 kJ/mol and of element 120 of 353.8 kJ/mol on gold, as well as on other metals, were determined (Fig. 22). Finally, no proportionality was found between the $\Delta H_{sub}(M)$ and $-\Delta H_{ads}{}^{Au}(M)$ in group 1, because these quantities change in opposite directions with Z in these groups. In group 2, there is a correlation between $\Delta H_{sub}(M)$ and $-\Delta H_{ads}{}^{Au}(M)$.

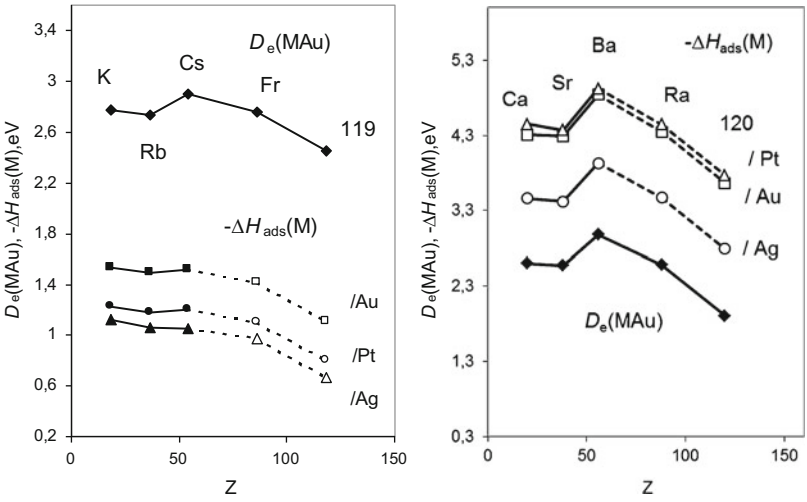


**Fig. 22** The 4c-DFT dissociation energies, $D_e$(MAu), and adsorption enthalpies $-\Delta H_{ads}(M)$ on Au, Pt, and Ag of group-1 elements and group-2 elements (*filled symbols* are semiempirical calculations, while open ones are obtained via correlations with $D_e$(MAu) (Reprinted with permission from Refs. [99] and [100]. Copyright 2012 Elsevier and 2013 American Institute of Physics, respectively)

The predicted $\Delta H_{ads}{}^{Au}(M)$ mean, however, that very high temperatures must be applied to establish an equilibrium $T_{ads}$. This is presently not feasible, because the detectors cannot be heated above $\sim 35\,^{\circ}C$.

Few other simple compounds of elements 119 and 120 were calculated, whose description can be found elsewhere [5, 8–11].

**Elements with Z > 120**. The chemistry of elements heavier than $Z = 120$ rests on a purely theoretical basis. Due to even stronger relativistic effects, as well as the existence of a plenty of open shells and their mixing, it will be much more different than anything known before. Very few molecular calculations exist in this SHE domain. The latest considerations of the chemistry of some of these elements can be found in [103, 104]. In this area, some unexpected oxidation states and coordination number like, e.g., $(E148)O_6$ or $(E158)X_8$ (X = halogen), could be reached.

## Aqueous Chemistry

- Redox potentials and stability of oxidation states

Knowledge of redox potentials, $E^{\circ}$, is very important for chemical separation of SHE. Early predictions of oxidation states and $E^{\circ}$ of the heaviest elements based on atomic DF and DS calculations and a Born-Haber cycle are summarized in [6]. Later, $E^{\circ}$ of Rf, Db, and Sg were estimated using results of atomic MCDF calculations of multiple IPs and known experimental redox potentials in group 4, 5, and 6 [48, 49]; see also [5, 8, 9] for reviews. The following trends were established for SHE: the stability of the maximum oxidation state increases within group 4 through 6 as a result of the proximity of the relativistically destabilized 6d AOs, while that of lower oxidation states decreases. Along the 7th period, the stability of the maximum oxidation state decreases: $E^{\circ}(Lr^{3+}/Lr^{2+}) < E^{\circ}(Rf^{IV}/Rf^{3+}) < E^{\circ}(Db^{V}/Db^{IV}) < E^{\circ}(Sg^{VI}/Sg^{V})$. A similar trend is observed for $E^{\circ}(M^{Zmax}/M)$. The increasing stability of the maximum oxidation state in group 4, 5, and 6 was shown to be a relativistic effect due to the proximity of the relativistic energy levels, while the 3+ state of Db and the 4+ state of Sg should be unstable. A summary of the redox potentials is given in Table 3.22 of [9].

- Complex formation and extraction by liquid chromatography

A number of theoretical works were devoted to predictions of complex formation, hydrolysis, and extraction behavior of Rf, Db, and Sg, in aqueous acid solutions (Eq. 5). Complex formation of Hs has also been studied as a specific case. (See [5, 8, 9] for the reviews.) The predictions were made with the use of a model that treats the formation energy of a compound as a sum of ionic and covalent constituents. The latter were obtained via 4c-DFT electronic structure calculations of the systems of interest [105, 106]. Those studies demonstrated that even though

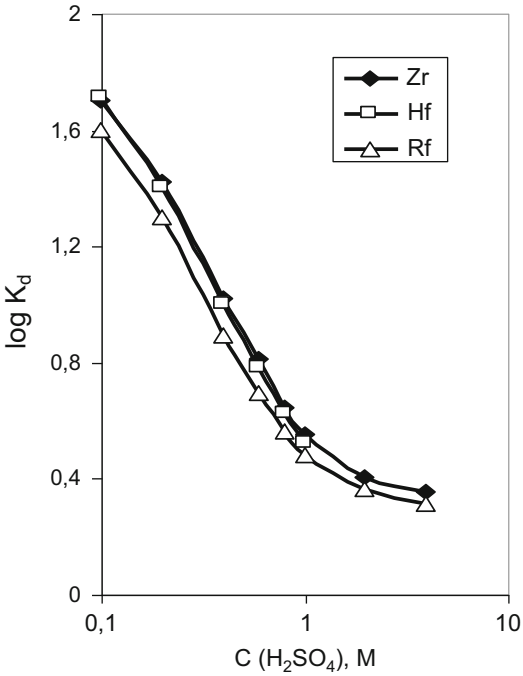


**Fig. 23** Predicted $\log K_d$ for the extraction of Hf and Rf by amines with respect to the measured ones for Zr (Reprinted with permission from Ref. [107]. Copyright 2006 Oldenbourg Wissenschaftsverlag GmbH)

the heaviest elements are homologs of their lighter congeners in the chemical groups, trends are not necessarily continued with them (see, e.g., predictions of an unexpected trend in the distribution coefficients, $K_d$, of the group-5 complexes by extraction from the HCl solutions into amines [105], confirmed by experiments [19]). The calculations have also shown that the theory of hydrolysis based on the ratio of the cation size to its charge does not explain, e.g., the difference between Nb and Ta or Mo and W. Only by performing relativistic calculations of the real chemical equilibria can the complex formation or hydrolysis be correctly predicted.

As an example, predictions of $\log K_d$ for the extraction of Zr, Hf, and Rf from the $H_2SO_4$ solutions by amines are shown in Fig. 23. For that purpose, the formation energies of the $M(SO_4)_2(H_2O)_4$, $M(SO_4)_3(H_2O)_2^{2-}$, and $M(SO_4)_4^{4-}$ (M = Zr, Hf, and Rf) complexes were calculated using the 4c-DFT method [107]. According to the results, the following trend in the complex formation was predicted: Zr > Hf $\gg$ Rf. Aqueous chemistry extraction experiments [108] confirmed the theoretically predicted trend and have given the $K_d$(Rf) values close to the predicted ones.

A summary of the predicted trends in hydrolysis, complex formation, and extraction of the group-4 through group-6 elements including the heaviest is given in [5,8,9]. As one can see there, most of the predictions have been confirmed by the experiments, while some of them, e.g., predictions for Sg in HF solutions [109], are still awaiting the confirmation.

## Summary

Theoretical studies on the electronic structures and properties of SHE have reached in the recent years remarkable achievements. With many of them linked to the experimental research, these investigations have contributed to better understanding of chemistry of these exotic elements, as well as the role and magnitude of relativistic effects. They helped predict the outcome of sophisticated and demanding experiments with single atoms and interpret their results.

Atomic structures were accurately predicted at the DCB CCFS level of theory for elements up to Z = 122. For the heavier elements, there is still some uncertainty in the ground states, so that the structure of the 8th row of the periodic table is still being discussed and debated.

Molecular calculations were performed for Rf through Z = 118 and a few heavier elements using a variety of relativistic methods, from DF CC ab initio to quasi-relativistic schemes. Most valuable information about properties of chemically interesting compounds (complex molecules, clusters, and solid state) was obtained with the use of the 4c-/2c-DFT and RECP/PP CC methods. They proved to be complimentary both conceptually and quantitatively, and their combination is the best way to investigate properties of the heaviest elements.

It was shown that elements Rf through 118 are homologs of their lighter congeners in the chemical groups, though their properties may differ due to very large relativistic effects. Straightforward extrapolations in the chemical groups can, therefore, result in erroneous predictions. For even heavier elements, properties should be even more unusual due to the mixing of many electronic states.

In the future, theoretical chemistry will still have a number of exciting tasks with respect to the new systems under investigation. Some further methodical developments in the relativistic quantum theory, like, e.g., inclusion of the QED effects on the SCF basis in molecular calculations, will be needed to achieve a required accuracy of the calculations.

**Acknowledgements** The author thanks her former collaborators J. Anton, T. Bastug, E. Eliav, U. Kaldor, and A. Borschevsky for the fruitful joint work. She also appreciates valuable discussions of the experimental results with her colleagues A. Yakushev, J.V. Kratz, Ch. E. Düllmann, and A. Türler.

## References

1. Schädel M, Shaughnessy D (eds) (2014) The chemistry of the superheavy elements, 2nd edn. Springer, Heidelberg
2. Moody KJ (2014) Synthesis of superheavy elements. In: Schädel M, Shaughnessy D (eds) The chemistry of the superheavy elements, 2nd edn. Springer, Heidelberg, pp 1–82
3. Oganessian YuTs (2011) Synthesis of the heaviest elements in $^{48}$Ca-induced reactions. Radiochim Acta 99:429–440
4. http://www.IUPAC.org: Discovery and assignment of elements with atomic numbers 113, 115, 117 and 118, 30 Dec 2015; Update 21 Jan 2016: technical reports available

5. Türler A, Pershina V (2013) Advances in the production and chemistry of the heaviest elements. Chem Rev 113:1237–1312
6. Fricke B (1975) Superheavy elements. A prediction of their chemical and physical properties. Struct Bond 21:89–144
7. Seaborg GT (1996) Evolution of the modern periodic table. J Chem Soc Dalton Trans 3899–3907
8. Hoffman DC, Lee DM, Pershina V (2006) Transactinide elements and future elements. In: Morss LR, Edelstein NM, Fuger J (ed) The chemistry of the actinide and transactinide elements, 3rd edn. Springer, Dordrecht, Ch 14, pp 1652–1752
9. Pershina V (2014) Theoretical chemistry of the heaviest elements. In: Schädel M, Shaughnessy D (eds) The chemistry of the superheavy elements, 2nd edn. Springer, Heidelberg, pp 135–240
10. Schwerdtfeger P, Seth M (1998) Relativistic effects on the superheavy elements. In: von Rague Schleyer P (ed) Encyclopedia on calculational chemistry, vol 4. Wiley, New York, pp 2480–2499
11. Pershina V (2011) Relativistic electronic structure studies on the heaviest elements. Radiochim Acta 99:459–476
12. Desclaux JP (1973) Relativistic Dirac-Fock expectation values for atoms with Z=1 to Z=120. At Data Nucl Data Tables 12:311–386
13. Eliav E, Kaldor U (2002) Four-component electronic structure methods. In: Schwerdtfeger P (ed) Relativistic electronic structure theory, Parts I and 2. Elsevier, Amsterdam, Part II, pp 279–350
14. Pyykkö P, Tokman M, Labzowsky LN (1998) Estimated valence-level Lamb shifts for group 1 and group 11 metal atoms. Phys Rev A 57:R689–692
15. Goidenko I, Labsowsky L, Eliav E, Kaldor U, Pyykkö P (2003) QED corrections to the binding energy of the eka-radon (Z=118) negative ion. Phys Rev A 67:020102(R)
16. Thierfelder C, Schwerdtfeger P (2010) Quantum electrodynamic corrections for the valence shell in heavy many-electron atoms. Phys Rev A 82:062503
17. Zvara I (2008) The inorganic radiochemistry of heavy elements. Springer, Berlin
18. Gäggeler HW, Türler A (2014) Gas-phase chemistry of superheavy elements. In: Schädel M, Shaughnessy D (eds) The chemistry of the superheavy elements, 2nd edn. Springer, Heidelberg, pp 415–484; Türler A, Gregorich KE (2003) Experimental techniques. *Ibid*: pp 261–308; also In: Schädel M (ed) The chemistry of superheavy elements, 1st edn. Kluwer Academic Publishers, Dordrecht, p 318
19. Kratz JV, Nagame J (2014) Liquid-phase chemistry of superheavy elements. In: Schädel M, Shaughnessy D (eds) The chemistry of the superheavy elements, 2nd edn. Springer, Heidelberg, pp 309–374
20. Schwerdtfeger P (ed) (2002) Relativistic electronic structure theory. Parts I and 2. Elsevier, Amsterdam
21. Barysz M, Ishikawa Y (ed) Relativistic methods for chemists. Springer, Dordrecht (2010)
22. Sucher J (1980) Foundation of the relativistic theory of many-electron atoms. Phys Rev A 22:348–362
23. Liu W (2014) Advances in relativistic molecular quantum mechanics. Phys Rep 537:59–89
24. Visscher L (2002) Post-Dirac-Fock methods. In: Schwerdtfeger P (ed) Relativistic electronic structure theory, Part I. Elsevier, Amsterdam, pp 291–331
25. Saue T (2002) Post Dirac-Fock-methods-properties. In: Schwerdtfeger P (ed) Relativistic electronic structure theory, Part I. Elsevier, Amsterdam, pp 332–397
26. DIRAC, a relativistic ab initio electronic structure program, written by Jensen AaHJ, Saue T, Visscher L et al. http://dirac.chem.sdu.dk
27. Douglas M, Kroll NM (1974) Quantum electrodynamical corrections to the fine structure of hellium. Ann Phys 82:89–155
28. Kutzelnig W, Liu W (2005) Quasirelativistic theory equivalent to fully relativistic theory. J Chem Phys 123:241102-4
29. Liu W (2010) Ideas of relativistic quantum theory. Mol Phys 108:1679–1706

30. Liu W, Peng D (2009) Exact two-component Hamiltonian revisitred. J Chem Phys 131:031104-4
31. Ilias M, Saue T (2007) An infinite-order two-component relativistic Hamiltonian by a simple one-step transformation. J Chem Phys 126:064102-9
32. Barysz M (2010) Two-component relativistic theories. In: Barysz M, Ishikawa Y (ed) Relativistic methods for chemists. Springer, Dordrecht, pp 165–190
33. Dolg M (2002) Relativistic effective core potentials. In: Schwerdtfeger P (ed) Relativistic electronic structure theory, Part 1. Elsevier, Amsterdam, pp 793–862
34. Schwerdtfeger P (2011) The pseudopotential approximation in electronic structure theory. Chem Phys Chem 12:3143–3155
35. Lee YS (2002) Two-component relativistic effective core potential calculations for molecules. In: Schwerdtfeger P (ed) Relativistic electronic structure theory, Part II. Elsevier, Amsterdam, pp 352–416
36. Nash CS, Bursten BE, Ermler WC (1997) Ab initio relativistic effective potentials with spin-orbit operators. VII. Am through element 118. J Chem Phys 106:5153–5145
37. Mosyagin NS, Petrov AN, Titov AV, Tupitsyn II (2006) In: Julien JP (ed) Recent advances in the theory of chemical and physical systems. Springer, Dordrecht, pp 229–251
38. Koch W, Holthausen MC (eds) (2000) A chemist's guide to density functional theory. Wiley-VCH, Weinheim
39. Anton J, Fricke B, Engel E (2004) Noncollinear and collinear relativistic density-functional program for electric and magnetic properties of molecules. Phys Rev A 69:012505(10)
40. Liu W, Hong, G, Dai D, Li L, Dolg M (1997) The Beijing four-component density functional program package (BDF) and its application to EuO, EuS, YbO, and YbS. Theor Chem Acc 96:75–83
41. ReSpect, version 3.3.0. Relativistic Spectroscopy DFT program of authors Repisky M, Komorovsky S, Malkin VG, Malkina OL, Kaupp M, Ruud K, with contributions from Bast R, Ekstrom U, Knecht S, Malkin Ondik I, Malkin E. (2013). http://rel-qchem.sav.sk
42. Liu W, Peng D (2006) Infinite-order quasirelativistic density functional method based on the exact matrix quasirelativistic theory. J Chem Phys 125:044102-10; Peng D, Liu W, Xiao Y, Cheng L (2007) Making one- and two-component density-functional methods fully equivalent based on the idea from atoms to molecules. J Chem Phys 127:104106-4
43. Van Wüllen C (2002) Relativistic density functional calculations on small molecules. In: Schwerdtfeger P (ed) Relativistic electronic structure theory, Part II. Elsevier, Amsterdam, pp 598–655
44. ADF, theoretical chemistry, Vrije Universiteit Amsterdam, The Netherlands. http://www.scm.com
45. Hess BA (1986) Relativistic electronic structure calculations employing a two-component no-pair formalism with external-field projection operators. Phys Rev A 33:3742–3748
46. Koepernik K, Eschrig H (1999) Full-potential nonorthogonal local-orbital minimum-basis band-structure scheme. Phys Rev B 59:1743–1757. http://www.FPLO.de
47. Pershina V, Bastug T (2005) Relativistic effects on experimentally studied gas-phase properties of the heaviest elements. Chem Phys 311:139–150
48. Johnson E, Fricke B, Keller OL Jr, Nestor CW Jr, Tucker TC (1990) Ionization potentials and radii of atoms and ions of element 104 (unnilquadium) and of hafnium (2+) derived from multiconfiguration Dirac-Fock calculations. J Chem Phys 93:8041–8050
49. Johnson E, Fricke B, Jacob T, Dong CZ, Fritzsche S, Pershina V (2002) Ionization potentials and radii of neutral and ionized species of elements 107 (bohrium) and 108 (hassium) from extended multiconfiguration Dirac-Fock calculations. J Phys Chem 116: 1862–1868
50. Nefedov VI, Yarzhemcky VG, Trzhaskovskaya MB (2004) Periodic low as applied to superheavy elements: specific features arising from relativistic effects. Russ J Inorg Chem 49:1871
51. Nefedov VI, Trzhaskovskaya MB, Yarzhemcky VG (2006) Electronic configurations and the periodic table for superheavy elements. Dokl Phys Chem 408:149

52. Indelicato P, Bieron J, Jönnson P (2011) Are MCDF calculations 101% correct in the superheavy element range? Theor Chem Acc 129:495–505
53. Pyykko P (2011) A suggested periodic table up to $Z \leq 172$, based on Dirac-Fock calculations on atoms and ions. Phys Chem Chem Phys 13:161–168
54. Liu W, Dolg M, Schwerdtfeger P. Benchmark relativistic all-electron density functional and ab initio pseudopotential study of group 12 dimers $M_2$ (M = Zn, Cd, Hg and eka-Hg). Unpublished
55. Seth M, Schwerdtfeger P, Dolg M (1997) The chemistry of the superheavy elements. I. Pseudopotentials for 111 and 112 and relativistic coupled cluster calculations for $(112)H^+$, $(112)F_2$, and $(112)F_4$. J Chem Phys 106:3623
56. Nash CS (2005) Atomic and molecular properties of elements 112, 114 and 118. J Phys Chem A 109:3493–3500
57. Pershina V, Borschevsky A, Eliav E, Kaldor U (2008) Prediction of the adsorption behavior of elements 112 and 114 on inert surfaces from ab initio Dirac-Coulomb atomic calculations. J Chem Phys 128:024707
58. Eliav E, Kaldor U, Ishikawa Y (1995) Transition energies in mercury and eka-mercury (element 112) by the relativistic coupled-cluster method. Phys Rev A 52:2765
59. Haynes WM (ed) (2012–2013) CRC handbook of chemistry and physics, 93rd edn. Taylor & Francis Ltd, London
60. Pershina V, Borschevsky A, Eliav E, Kaldor U (2008) Adsorption of inert gases including element 118 on noble metal and inert surfaces from ab initio Dirac–Coulomb atomic calculations. J Chem Phys 129:144106
61. Borschevsky A, Pershina V, Eliav E, Kaldor U (2009) Electron affinity of element 114, with comparison to Sn and Pb. Chem Phys Lett 480:49–51
62. Borschevsky A, Pershina V, Eliav, Kaldor U (2013) Ab initio predictions of atomic properties of element 120 and its lighter group-2 homologues. Phys Rev A 87:022502(8)
63. Pyykkö P, Atsumi M (2009) Molecular single-bond covalent radii for elements 1-118. Chem Eur J 15:186–197; Pyykkö P, Riedel S, Patzsche M (2005) Triple-bond covalent radii. *ibid* 11:3511–3620
64. Pershina V, Borchsevsky A, Ilias M (2014) Theoretical predictions of properties and volatility of chlorides and oxychlorides of group-4 elements. I. Electronic structure and properties of $MCl_4$ and $MOCl_2$ (M = Ti, Zr, Hf, and Rf). J Chem Phys 141:064314(8)
65. Pershina V, Borchsevsky A, Ilias M, Türler A (2014) Theoretical predictions of properties and volatility of chlorides and oxychlorides of group-4 elements. II. Adsorption of tetrachlorides and oxydichlorides of Zr, Hf, and Rf on neutral and modified surfaces. J Chem Phys 141:064315(7)
66. Pershina V, Anton J (2012) Theoretical predictions of properties and gas-phase chromatography behaviour of bromides of group-5 elements Nb, Ta and element 105, Db. J Chem Phys 136:034308(7)
67. Türler A, Brücle W, Dressler R, Eichler B, Eichler R, Gäggeler HW, Gärtner M, Glatz J-P, Gregorich KE, Hübener S, Jost DT, Lebedev VYa, Pershina V, Schädel M, Taut S, Timokhin N, Trautmann N, Vahle A, Yakushev AB (1999) First measurements of a thermochemical property of a seaborgium compound. Angew Chem Int Ed 38:2212–2213
68. Pershina V, Fricke B (1996) Group-6 dioxydichlorides $MO_2Cl_2$ (M = Cr, Mo, W, and element 106, Sg): the electronic structure and thermochemical stability. J Phys Chem 100:8748–8751
69. Han YK, Son SK, Choi YJ, Lee YS (1999) Structures and stabilities for halides and oxides of transactinide elements Rf, Db, and Sg calculated by relativistic effective core potential methods. J Phys Chem A 103:9109–9115
70. Even J, Yakushev A, Düllmann ChE, Haba H, Asai M, Sato TK, Brand H, Di Nitto A, Eichler R, Fan FL, Hartmann W, Huang M, Jäger E, Kaji D, Kanaya J, Kaneya Y, Khuyagbaatar J, Kindler B, Kratz JV, Krier J, Kudou Y, Kurz N, Lommel B, Miyashita S, Moritomo K, Morita K, Murakami M, Nagame Y, Nitsche H, Ooe K, Qin Z, Schädel M, Steiner J, Sumita T, Takeyama M, Tanaka K, Toyoshima A, Tsukada K, Türler A, Usoltsev I, Wakabayashi Y, Wang Y, Wiehl N, Yamaki S (2014) Synthesis and detection of a seaborgium carbonyl complex. Science 345:1491–1493

71. Nash CS, Bursten BE (1999) Prediction of the bond lengths, vibrational frequencies, and bond dissociation energy of octahedral seaborgium hexacarbonyl, $Sg(CO)_6$. J Am Chem Soc 121:10830–10831
72. Pershina V, Anton J (2013) Theoretical predictions of properties and gas-phase chromatography behaviour of carbonyl complexes of group-6 elements Cr, Mo, W, and element 106, Sg. J Chem Phys 138:174301(6)
73. Eichler R, Brüchle W, Dressler R, Düllman ChE, Eichler B, Gäggeler HW, Gregorich KE, Hoffman DC, Hübener S, Jost DT, Kirbach UW, Laue CA, Lavanchy VM, Nitsche H, Patin JB, Piguet D, Schädel M, Shaughnessy DA, Strellis DA, Taut S, Tobler L, Tsyganov YS, Türler A, Vahle A, Wilk PA, Yakushev AB (2000) Chemical characterization of bohrium (element 107). Nature 407:63–65
74. Pershina V, Bastug T (2000) The electronic structure and properties of group 7 oxychlorides, $MO_3Cl$, where M = Tc, Re, and element 107, Bh. J Chem Phys 113:1441–1446
75. Düllmann ChE, Brüchle W, Dressler R, Eberhardt K, Eichler B, Eichler R, Gäggeler HW, Ginter TN, Glaus F, Gregorich K, Hoffman DC, Jäger E, Jost DT, Kirbach UW, Lee DE, Nitsche H, Patin JB, Pershina V, Piguet D, Qin Z, Schädel M, Schausten B, Schimpf E, Schött HJ, Soverna S, Sudowe R, Thörle P, Timokhin SN, Trautmann N, Türler A, Vahle A, Wirth G, Yakushev AB, Zielinski PM (2002) Chemical investigation of hassium (element 108). Nature 418:859–862
76. Pershina V, Anton J, Jacob T (2008) Fully-relativistic DFT calculations of the electronic structures of $MO_4$ (M = Ru, Os, and element 108, Hs) and prediction of physisorption. Phys Rev A 78:032518(5)
77. Pitzer KS (1975) Are elements 112, 114, and 118 relatively inert gases? J Chem Phys 63:1032–1033
78. Eichler R, Aksenov NV, Belozerov AV, Bozhikov GA, Chepigin VI, Dmitriev SN, Dressler R, Gäggeler HW, Gorshkov VA, Haenssler F, Itkis MG, Laube A, Lebedev VYa, Malyshev ON, Oganessian YuTs, Petrushkin OV, Piguet D, Rasmussen P, Shishkin SV, Shutov SV, Svirikhin AI, Tereshatov EE, Vostokin GK, Wegrzecki M, Yeremin AV (2007) Chemical characterization of element 112. Nature. Letters 447:72–73
79. Borschevsky A, Pershina V, Eliav E, Kaldor U (2014) Relativistic couple cluster study of diatomic compounds of Hg, Cn, and Fl. J Chem Phys 141:084301-7
80. Liu W, van Wüllen Ch, Han YK, Choi YJ, Lee YS (2001) Spectroscopic constants of Pb and Eka-lead compounds: comparison of different approaches. Adv Quant Chem 39:325–355
81. Anton J, Fricke B, Schwerdtfeger P (2005) Non-collinear and collinear four-component relativistic molecular density functional calculations. Chem Phys 311:97–103
82. Pershina V, Anton J, Fricke B (2007) Intermetallic compounds of the heaviest elements and their homologs: the electronic structure and bonding of MM, where M = Ge, Sn, Pb, and element 114, and M = Ni, Pd, Pt, Cu, Ag, Au, Sn, Pb, and element 114. J Chem Phys 127:134310(9)
83. Gaston N, Opahle I, Gäggeler HW, Schwerdtfeger P (2007) Is eka-mercury (element 112) a group 12 metal? Angew Chem Int Ed 46:1663–1666
84. Pershina V, Bastug T, Fricke B, Jacob T, Varga S (2002) Intermetallic compounds of the heaviest elements: the electronic structure and bonding of dimers of element 112 and its homolog Hg. Chem Phys Lett 365:176–183
85. Sarpe-Tudoran C, Fricke B, Anton J, Pershina V (2007) Adsorption of superheavy elements on metal surfaces. J Chem Phys 126:174702(5)
86. Pershina V, Anton J, Jacob T (2009) Theoretical predictions of adsorption behavior of elements 112 and 114 and their homologs Hg and Pb. J Chem Phys 131:084713(8)
87. Zaitsevkii A, Titov A (2009) Relativistic pseudopotential model for superheavy elements: applications to chemistry of eka-Hg and eka-Pb. Russ Chem Rev 78:1173–1181
88. Zaitsevskii A, van Wüllen C, Rykova EA (2010) Two-component relativistic density functional modeling of the adsorption of element 114 (eka-led) on gold. Phys Chem Chem Phys 12:4152–4156
89. Eichler R, Aksenov NV, Albin YuV, Belozerov AV, Bozhikov GA, Chepigin VI, Dmitriev SN, Dressler R, Gäggeler HW, Gorshkov VA, Henderson RA, Johnsen AM, Kenneally JM,

Lebedev VYa, Malyshev ON, Moody KJ, Oganessian YuTs, Petrushkin OV, Piguet D, Popeko AG, Rasmussen P, Serov A, Shaughnessy DA, Shishkin SV, Shutov AV, Stoyer MA, Svirikhin AI, Tereshatov EE, Vostokin GK, Wegrzecki M, Wittwer PA, Yeremin AV (2010) Indication for a volatile element 114. Radiochim Acta 98:133–139

90. Yakushev A, Gates JM, Türler A, Schädel M, Düllmann ChE, Ackermann D, Andersson LL, Block M, Brüchle W, Dvorak J, Eberhardt K, Essel HG, Even J, Forsberg U, Gorshkov A, Graeger R, Gregorich KE, Hartmann W, Herzberg RD, Hessberger F, Hild D, Hübner A, Jäger E, Khuyagbaatar J, Kindler B, Kratz JV, Krier J, Kurz N, Lommel B, Niewisch J, Nitsche H, Omtvedt JP, Parr E, Qin Z, Rudolph D, Runke J, Schausten B, Schimpf E, Semchenkov A, Steiner J, Thörle-Pospiech P, Uusito J, Wegrzecki M, Wiehl N (2014) Superheavy element flerovium (element 114) is a volatile metal. Inorg Chem 53:1624–1629
91. Eichler B (1976) Das Flüchtigkeitsverhalten von Transactiniden im Bereich um Z = 114 (Voraussage). Kernenergie 19:307–311; Eichler B, Zvara I (1982) Evaluation of the enthalpy of adsorption from thermodynamic data. Radiochim Acta 30:233–238
92. Pershina V, Borschevsy A, Anton J, Jacob T (2010) Theoretical predictions of trends in spectroscopic properties of homonuclear dimers and volatility of the 7p elements. J Chem Phys 132:194314(11)
93. Pershina V, Borschevsy A, Anton J, Jacob T (2010) Theoretical predictions of trends in spectroscopic properties of gold containing dimers of the 6p and 7p elements and their adsorption on gold. J Chem Phys 133:104304(10)
94. Hermann A, Furthmüller J, Gäggeler HW, Schwerdtfeger P (2010) Spin-orbit effects in structural and electronic properties for the solid state of the group-14 elements from carbon to superheavy element 114. Phys Rev B 82:155116(8)
95. Pershina V, Anton J, Jacob T (2009) Electronic structures and properties of MAu and MOH, where M = Tl and element 113. Chem Phys Lett 480:157–160
96. Fox-Beyer BS, van Wüllen C (2012) Theoretical modelling of the adsorption of thallium and element 113 atoms on gold using two-component density functional methods with effective core potentials. Chem Phys 395:95–103
97. Serov A, Eichler R, Dressler R, Piguet D, Türler A, Vögele A, Wittwer D, Gäggeler HW (2013) Adsorption interaction of carrier-free thallium species with gold and quartz surfaces. Radiochim Acta 101:421–426
98. Nash CS, Bursten BE (1999) Spin-orbit coupling versus the VSEPR method: on the possibility of a nonplanar structure for the super-heavy noble gas tetrafluoride (118)$F_4$. Angew Chem Int Ed 38:151–153
99. Pershina V, Borschevsky A, Anton J (2012) Fully relativistic study of intermetallic dimers of group-1 elements K through element 119 and prediction of their adsorption on noble metal surfaces. Chem Phys 395:87–94
100. Pershina V, Borschevsky A, Anton J (2012) Theoretical predictions of properties of group-2 elements including element 120 and their adsorption on noble metal surfaces. J Chem Phys 136:134317(10); *ibid* (2013) 139:239901
101. Demidov Y, Zaitsevskii A, Eichler R (2014) First principles based modelling of the adsorption of atoms of element 120 on a gold surface. Phys Chem Chem Phys 16:2268–2270
102. Eichler B, Rossbach H (1983) Adsorption of volatile metals on metal surfaces and its application in nuclear chemistry. Radiochim Acta 33:121–125
103. Pyykkö P (2012) The physics behind chemistry and the periodic table. Chem Rev 112:371–384
104. Pyykkö P (2012) Predicting new, simple inorganic species by quantum-chemical calculations: some successes. Phys Chem Chem Phys 14:14734–14737
105. Pershina V (1998) Part II: hydrolysis and complex formation of Nb, Ta, Ha and Pa in HCl solutions. Radiochim Acta 80:75–84
106. Pershina V, Kratz JV (2001) Solution chemistry of element 106: theoretical predictions of hydrolysis of group 6 cations Mo, W, and Sg. Inorg Chem 40:776–780
107. Pershina V, Polakova D, Omtvedt JP (2006) Theoretical predictions of complex formation of group-4 elements Zr, Hf, and Rf in $H_2SO_4$ solutions. Radiochim Acta 94:407–414

108. Li ZJ, Toyoshima A, Tsukada K, Nagame Y (2010) Ion-exchange behavior of Zr and Hf as homologues of element 104, Rf, in $H_2SO_4$ and $H_2SO_4/HClO_4$ mixed solutions. Radiochim Acta 98:7–12
109. Pershina V (2004) Theoretical treatment of the complexation of element 106, Sg, in HF solutions. Radiochim Acta 92:455–462